Development of a miniature AC Susceptometer for a Cryogenic System

UNIVERSIDADE DE COIMBRA

Francisco José Pires de Almeida

Department of Physics

University of Coimbra

This dissertation is submitted for the degree of

Master in Engeneering Physics

September 2015

I would like to dedicate this thesis to my loving parents ...

Acknowledgements

Firstly, I would like to express my sincere gratitude to my supervisor, Professor José António Paixão for the availability while developing the project. For his patience, motivation, and vast knowledge.

I would like to thank Marta for the companionship during this year.

A shout of gratitude to Eng. Nuno Lucas, who presented availability and help when the need raised.

In addition I would like to thank to all my family and friends who helped me to be what I am today.

Access to TAIL-UC facility funded under QREN-Mais Centro project ICT_2009_02_012_1890 is gratefully acknowledged.

Resumo

Neste trabalho é descrito o desenvolvimento de um Susceptómetro AC para um crióstato que opera entre 10 e 300K.

Amostras de YBaCuO e de UFe_4Al_8 foram testadas no nosso susceptómetro AC e num magnetometro comercial de forma a verificar propriedades que são detectadas am ambos os sistemas para poder confirmar as medidas do susceptómetro AC.

O sistema apresenta baixo ruído, como esperado pelo uso de um amplificador de Lock-in, e foram conseguidos bons resultados, quando comparadas as medidade de susceptibilidade DC e AC.

Abstract

In this work is described the development of a miniature AC Susceptometer for a cryogenic system operating in a temperature range between 10 and 300 K.

A sample of YBaCuO and another of UFe_4Al_8 were tested in our AC susceptometer and in a DC commercial magnetometer in order to ascertain common properties detected by both so the AC measurements can be confirmed.

The system presented very low noise, expected from the use of a Lock-in Amplifier and produced good results, when compared both measurements from DC an AC susceptometry.

Table of Contents

List of figures

List of tables

Nomenclature

Acronyms / Abbreviations

DAC Digital-to-Analog Converter

DSP Digital Signal Processor

SQUID Superconducting Quantum Interference Device

emf Electromagnetic Field

GM Gifford-McMahon

LIA Lock-in Amplifier

PID Proportional, Integral and Derivative

PLL Phase Locked Loop

PSD Phase Sensitive Detection

VSM Vibrating Sample Magnetometer

rms Root Mean Square

TTL Transistor-Transistor Logic

Chapter 1

Introduction

In the study of magnetic phenomena in materials AC susceptibility is an invaluable technique that enables highly sensitive and contactless measurements of samples of small dimensions.

Magnetic properties can be measured by either DC or AC methods, but there is no overlap in their functionalities, and the two methods complement each other since DC measures the static properties of a sample in an uniform field ($\frac{M}{H}$) while AC is sensitive to the dynamic properties ($\frac{dM}{dH}$) of the sample when under an oscillating applied magnetic field. The sensitivity of the AC method typically surpasses that of DC techniques, but calibration is quite difficult as the measured data is the derivative of the magnetization.

Today, commercial AC susceptometers can be found, but are too expensive. Many laboratories prefer to develop home made susceptometers, and such instruments can still attain sensitivity ($\sim$ 100 times) higher than in DC methods.

While building an AC susceptometer there is the need into take to account the system specifications, such as the space available for the susceptometer, the foreseen system capabilities, and the samples that will be measured. The configuration used for the susceptometer coils is mostly consensual, but alternative coil designs [6] for large bulk samples or very small ones [9] have been developed.

1.1 Motivation

The motivation for this project came from the need to complement the DC magnetometry equipment at the Physics Department with an AC instrument. As the commercial solutions are very expensive, the challenge of this project was to develop our own instrument using equipment already existing at our disposal, to minimize costs. One such piece of equipment was a lock-in amplifier that was put to good use in the AC susceptometer. The possibility to work with a Lock-in amplifier was particularly interesting because such instrument is widely

used in several fields of metrology, and as lock-in amplifiers are not studied in detail in my undergraduate studies it was an additional motivation for this project.

1.2 State of the art

Magnetic AC susceptibility measurements have been performed for a long time and the birth of the technique is not well documented. Systems working without phase sensitive detection were very prone to pick up noise but the modern design has overcome this problem. The revolution happened around the 50's when the Lock-in Amplifier was developed in Princeton University, enabling sensitive measurements within narrow frequency bands, cleaning retrieving the measured signal out of the unavoidable electrical laboratory noise.

The glory days of AC susceptibility came after 1985, when high-T_C superconductors where discovered as this technique is ideal for the characterization of superconductors.

At the present time, highly performant commercial AC susceptometers have been developed with innovative designs such as adding to the pick-up coils an extra pair of compensation and calibration coils [11].

Very recently a home made miniature AC susceptometer was reported by Yonezawa, et al [15] with a similar design to ours but coupled to an Adiabatic Demagnetization Refrigerator capable of attaining temperatures as low as 100 mK. This can be considered the current state of the art.

1.3 System Specifications

The initial goals of this project comprised the design, construction, calibration and testing of a miniature AC magnetic susceptometer that should fulfil the following specifications:

- Primary/sensing coil set of reduced dimensions in order to fit in the cold finger of a closed cycle helium cryostat;
- Working temperature range from 10-300 K;
- Frequency range from 30-100000 Hz;
- High sensitivity such as to detect signals from ferromagnetic samples as small as $\sim 1\text{mm}^3$. In order to detect very small signals from such tiny samples, the design comprised lock-in phase sensitive detection and amplification (using a SR830 Lock-in Amplifier);

- Full computerized control of all devices;
- Flexible software control written in a high-level scripting language capable of running user defined measurement sequences and macros;
- Real-time graphical representation of the relevant measured data. By design, and in the sake of flexibility and robustness of the data acquisition system the graphics display should not be hard-coupled to the control program but rather communicating with it in a client/server protocol.

1.4 Plan of work

The plan of this project was the following:

- Design and construction of the coil system;
- Implementation of the coils in the cold finger of a commercial closed cycle helium cryostat;
- Design and implementation of the data acquisition system around an SR830 Lock-in Amplifier that should act as detection system as well as feeding the primary coils;
- Software development according to the specification including writing up all the necessary drivers to communicate with the equipment;
- Calibration and test of the system.

The whole apparatus should use equipment already available at our disposal, such as a computer, a lock-in amplifier, a cryostat and a temperature controller to minimize the cost of the system.

Fine tuning of the system to achieve maximum performance was performed using test samples. These samples that are well documented tested not only the sensitivity of the magnetic measurements but also, and equally important, the accuracy of the thermometry of our instrument.

Chapter 2

Magnetism and Magnetic Properties

Materials present many physical properties that find use in a wide range of applications. These properties are studied to characterize a material that can be then selected with very distinctive uses in mind. The experiments done for the characterization can be performed at the micro or macroscopic levels and extend to many different properties.

Among these properties, the ones studied in this work are the magnetic properties of materials. These materials are present in our daily life in many devices, gadgets and machines we commonly use. Magnetism is a property that shows up in different behaviours.

The most commonly known magnetic materials are the ferromagnets, that are simply called magnets due to their ability to attract a piece of iron or another permanent magnet nearby. Although this is the most commonly known type of magnetism, all materials present some kind of magnetic property or response to the presence of a magnetic field, sometimes stronger, sometimes almost non-existent.

Magnetic phenomena generally appear due to the motion of electrical charges, whether due to wires carrying electric currents or, at the atomic scale, electrons orbiting around atomic nucleus or spinning around their axis. Analysing macroscopically, these current loops are so small that can be treated as magnetic dipoles, and can sometimes cancel each other due to random orientation of atoms. [4]

Many magnetic effects have been discovered in the past decades, and have been extensively studied. Several experimental characterization methods where developed and improved to fit the high characterization requirements of such materials.

2.1 Magnetic Dipole

Considering the magnetic behaviour of materials, a classical comparison with a magnetic dipole can be established. A magnetic dipole is an elementary magnetic quantity that can be produced by the movement of electrically charged particles.

Another example can take the form of well know bar magnets that consist of one magnetic dipole, represented as a compass that possess a north and a south pole, instead of the positive and negative poles characteristic of electrical dipoles. In an analogous form, magnetic field lines represent the direction of the magnetic field of the dipole, represented in Fig.2.1.

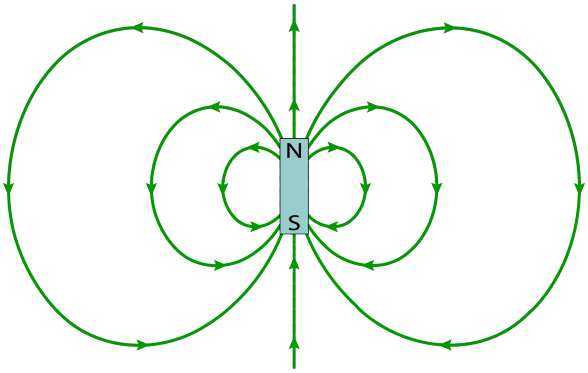

Fig. 2.1 Representation of the field lines of a magnetic dipole. [1]

Expanding this classical example, materials are composed of an infinite number of dipoles with finite number of moments, who define, summed all together, the magnetic field created by the material. Due to the high amount of dipoles present in any material and the interactions between neighbour dipoles, the total moment of the group can span a range from zero to a high value, depending on the magnetic behaviour of the sample.

2.2 Magnetic Field Vector

As previously mentioned, magnetic fields are, usually, generated by moving electrically charged particles, and, for that reason, a magnetic field can be created and controlled by an electric coil, where an electric current can flow, becoming the source of the field.

Coils can be designed and linked to a current source in order to control the magnetic field created. The relation between current in the coil and the magnetic field is:

$$\vec{H} = \frac{N}{l} I \, \vec{\eta} \tag{2.1}$$

[1] source by: http://www.thesciencemill.com/Research/edm/img/bar_magnet.png

where a magnetic field of strength H is created by a coil of N turns over length l when an electrical current $I = \frac{dq}{dt}$ flows through it.

Since the magnetic field is always induced in different environments, the way the magnetic field strength interacts with it comes as:

$$\vec{B} = \mu \vec{H} \tag{2.2}$$

and μ is the permeability of the environment and is related to the vacuum permeability by a ratio of the material permeability called relative permeability:

$$\mu = \mu_r \mu_0 \tag{2.3}$$

where μ_r is dimensionless and $\mu_0 = 4\pi\ 10^{-7}$ H/m, corresponding to the vacuum permeability.

As a current can produce a magnetic field, also a magnetic field can induce a current in a conductor. Such current can be used to measure the field.

2.3 Magnetization

The origin of magnetic moments in materials is a consequence of two atomic phenomena: orbital moment and the electron spin.

The orbital moment is due to the movement of the electron around the atomic nucleus providing the same effect as seen in the coil, a magnetic moment will be created, as depicted in Fig. 2.2.

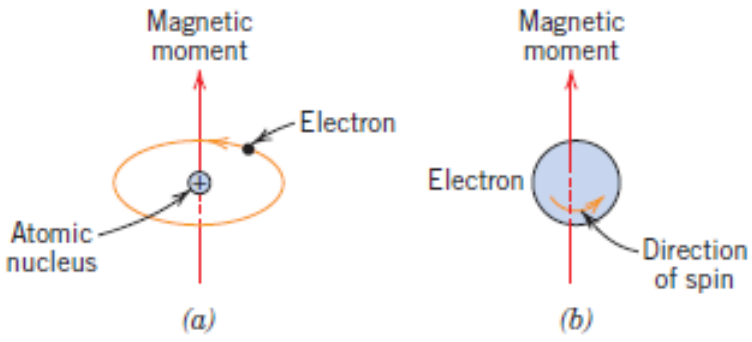

Fig. 2.2 Magnetic moment created by the (a) orbital moment of an electron and by the (b) electron spin. [2]

[2] source by: http://phys.thu.edu.tw/~hlhsiao/mse-web_ch20.pdf

The spin is an intrinsic magnetic moment of the electrons, irrespective of its motion and can only take two orientations (up or down) with respect to an external field. In closed-shell atoms, all the spin moments cancel, leaving the magnetic moment of the atoms to the orbital moment.

The magnetization, $\vec{M}$, of a material is the net magnetic dipole moment per unit volume:

$$\vec{M} = \frac{1}{V} \sum_i \vec{\mu}_i \tag{2.4}$$

This value is rather difficult to estimate by it self, because a sample is made of countless dipoles, all of them depend on the conditions the sample is subjected and because some materials might not present intrinsic permanent magnetization.

The magnetization adds up to the applied magnetic field that is induced by a coil, or some kind of field generator, as follows:

$$\vec{B} = \mu_0 \, (\, \vec{H} + \vec{M} \,), \tag{2.5}$$

where $\vec{B}$ is the magnetic field induction.

In many, but by no means all, materials, the magnetization is proportional to the field:

$$\vec{M} = \chi \, \vec{H} \tag{2.6}$$

where χ is a dimensionless variable that represents the magnetic susceptibility of the material and can take positive or negative values depending on the substance.

For such materials:

$$\vec{B} = \mu_0 \, (1 + \chi) \, \vec{H} \tag{2.7}$$

the permeability of the material is:

$$\mu = \mu_0 (1 + \chi) \tag{2.8}$$

and the relative permeability is

$$\mu_r = \frac{\mu}{\mu_0} = (1 + \chi). \tag{2.9}$$

2.4 Magnetism

From the concept of magnetic dipole and magnetization we shall now introduce the different magnetic behaviours that materials may present.

There are two basic magnetic behaviours, Diamagnetism and Paramagnetism, and from particular cases derived from the paramagnetic model, one can reach other three magnetic behaviours: Ferromagnetism, Antiferromagnetism and Ferrimagnetism.

2.4.1 Diamagnetism

Diamagnetism is a very weak form of magnetism, because the magnetization is not permanent, that means that it only persists while a magnetic field is applied to the diamagnetic material.

The behaviour of a diamagnetic material is to counteract the magnetic field applied, as shown in Fig. 2.3, where the material begins with a null magnetization.

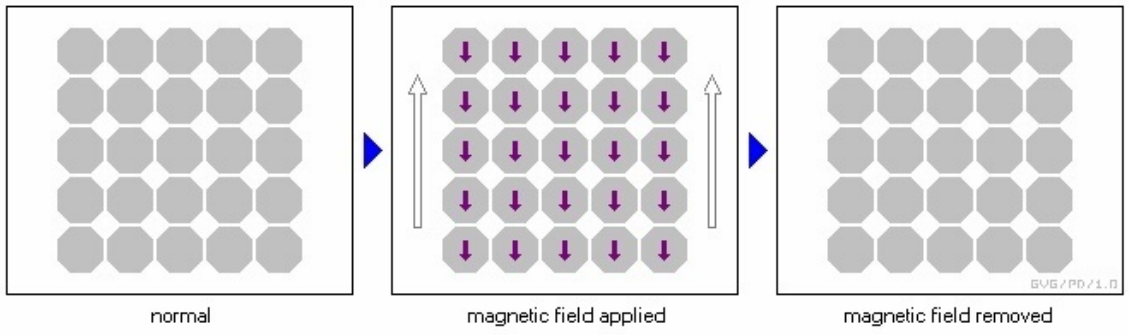

Fig. 2.3 Behaviour of a diamagnetic material to an applied magnetic field and its removal. [3]

When the magnetic field is removed, the total magnetization of the sample recovers its original state, showing the reversibility of the process.

As the total field, when the sample is subjected to an external magnetic field, is lower than the latter, according to Eq. 2.7, the susceptibility, χ, will be negative in such diamagnetic materials.

2.4.2 Paramagnetism

Paramagnetism is the simplest behaviour, where all the atoms possess a permanent dipole moment from incomplete electron cancellation, from orbital moment or electron spin moment.

The random atomic orientation, as depicted in Fig. 2.4, results in a null macroscopic magnetization at zero field and present a linear magnetization curve that describes a reversible process. [8]

[3] source by: http://www.madsci.org/posts/archives/2008-08/1219953614.Ph.3.jpg

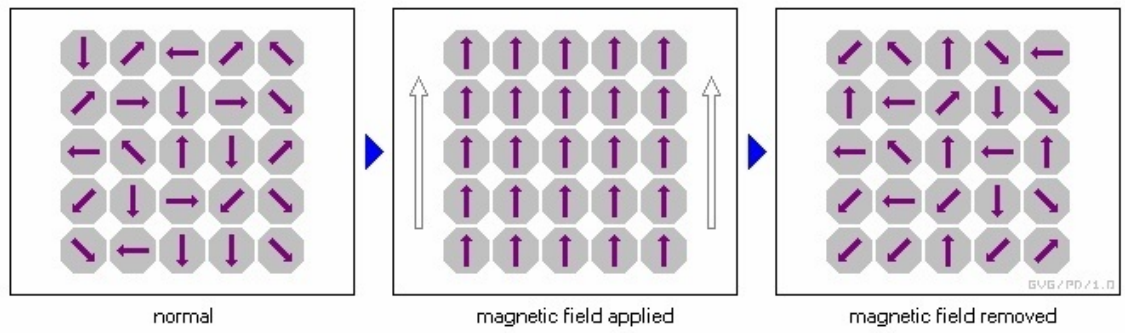

Fig. 2.4 Behaviour of a paramagnetic material to an applied magnetic field and its removal. [4]

Atomic dipoles from paramagnetic materials are not only random, but are free of interactions between themselves, meaning that there is no interaction between atomic magnetic moments and each one reacts individually to the applied field.

As they react seperatly to the magnetic field, any magnetic field applied will be enough to make atomic moments align to it, resulting in an increasing field. Opposite to diamagnetic materials, paramagnetic susceptibility is higher than zero.

2.4.3 Ferromagnetism

This is the strongest type of magnetism found in materials due to its permanent magnetization in the absence of a magnetic field, granting them the ability to attract pieces of iron, and that is why they are commonly called magnets.

Ferromagnets have a distinctive $M(H)$ curve, at a given temperature, that reveals a nonlinear and irreversible behaviour.

Contrary to paramagnetic materials, ferromagnet dipoles have coupling interactions that affect neighbour atoms influencing the orientation of the magnetic dipoles, showing a state of long range order and creating something called magnetic domains.

Magnetic domains are regions of material where dipoles have the same orientation and the coupling interactions maintain them as they are, and that is how ferromagnets are able to remain magnetized for longer periods of time than paramagnets, that randomly disorder back themselves after the magnetic field is suppressed.

One intrinsic property of these materials is remanence (magnetization in zero field after a magnetic field is applied and then suppressed), which is important because the magnetization doesn't reaches zero when the applied magnetic field vanishes. It is clearly an important characteristic of a ferromagnet.

[4] source by: http://i.stack.imgur.com/1hDbF.jpg

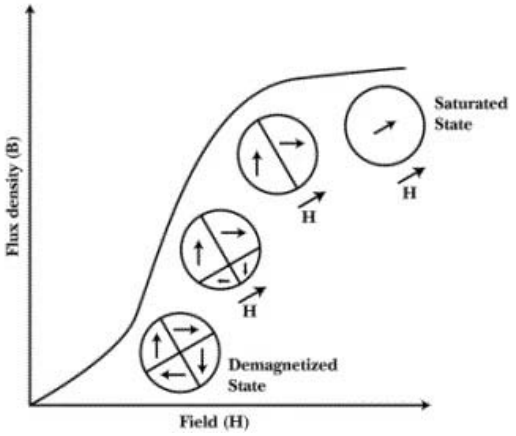

(a) Magnetization process of a ferromagnetic material and domain movement [5]

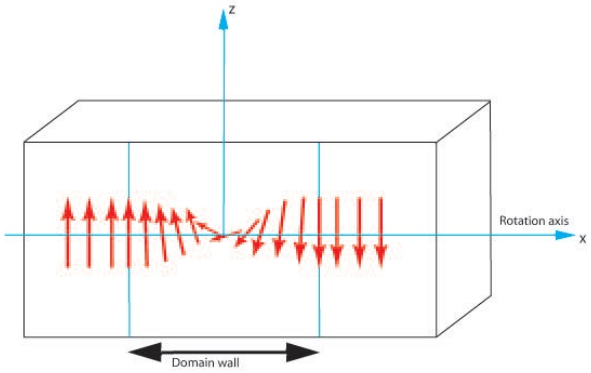

(b) Magnetic moment rotation in a domain wall [6]

Fig. 2.5 Magnetization process in ferromagnetic materials and domain wall.

Ferromagnetic materials also differ between soft and hard magnets, used for different purposes, because of distinct remanent magnetization and coercivities. Remanent magnetization and coercivities are not properties of a substance but rather dependent on the way the material has been produced and treated.

2.4.4 Antiferromagnetism

Antiferromagnetism is a property that sometimes leads to confusion because the name suggests a material comparable to a ferromagnet that reacts against the applied magnetic field with the magnetic moments aligned in the opposite direction.

In reality, the magnetic moments in antiferromagnets line up so the adjacent magnetic moments are aligned in opposite directions, forming a long range order state.

The values of magnetization in these materials are relatively small due to the moments being locked together in antiparallel alignment.

2.4.5 Ferrimagnetism

At a macroscopic level, ferrimagnetism behaves almost identically to a ferromagnet, showing $M(H)$ curves very similar to the latter and having the same kind of irreversible process of

[5] source by :http://www.doitpoms.ac.uk/tlplib/ferromagnetic/images/FigureP.gif

[6] source by :http://www.allegromicro.com/~/media/Images/Design/Dexter/figure1.ashx?w=332&h=280&as=1&la=en

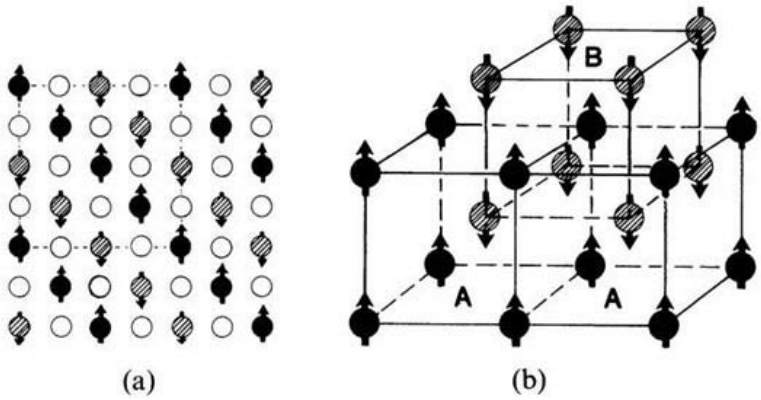

Fig. 2.6 Ordering of the magnetic moments in an antiferromagnetic material. [7]

magnetization. At a microscopic level it is similar to an antiferromagnetic material, having the same kind of coupling with antiparallel alignment.

This magnetic property differs from antiferromagnetism because adjacent atoms have different magnitudes, where higher magnetic moment dipoles tend to align with the applied field, and the smaller in the opposite direction.

[7] source by: http://what-when-how.com/wp-content/uploads/2011/07/tmp8361_thumb2.jpg

Chapter 3

Magnetometry

Magnetometry referrers to magnetic measurements and techniques (DC and AC) used to that end. DC and AC techniques don't overlap in functionality, since both have different operation procedure, studying the response of magnetic materials under different conditions and, with that, collecting different information about material properties.

3.1 DC Magnetometry

DC measurements determine the equilibrium magnetization of a sample when a DC field, H_{dc}, is applied, producing a DC magnetization curve dependent on that same applied field, $M(H_{dc})$. In this experiments a detection coil is used, to detect the change in the magnetic flux induced by the created field, with a system capable of moving the sample.

The DC, or static, susceptibility is then given by:

$$\chi_{dc} = \frac{M}{H_{dc}}. \tag{3.1}$$

These experiments generally use small samples and are able to generate relatively high magnetic fields.

Two typical instruments for DC magnetometry are the Vibrating Sample Magnetometer (VSM) and the Superconducting Quantum Interference Device ($SQUID$) Magnetometer.

3.1.1 VSM

The most common setup for VSM instruments is depicted in Fig. 3.1, where a pair of detection coils mounted inside an electromagnet that produces a uniform magnetic field, while the sample is attached to a vibrating sample holder that oscillates along the z-axis.

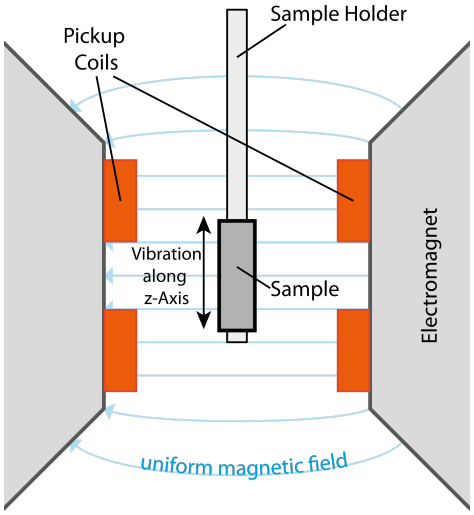

Fig. 3.1 VSM magnetometer common setup diagram. [8]

When magnetized, the sample's magnetic flux moves with the sample, while it oscillates, producing changes in the magnetic flux measured by the coils. The coils are connected and located so that, ideally, the signal due to the moving sample adds and any signal due to fluctuations of the field from the electromagnet subtracts and gets cancelled.

The vibration module is driven by a loudspeaker or equivalent mechanism connected to a small coil placed in the field of a permanent magnet. This method is simple and allows wide frequency range, however, the vibration amplitude can vary dependent on the sample mass, forcing the system to possess another set of reference coils in order to maintain and rectify any error in the sample vibration so reproducible measurements can be achieved. [3]

3.1.2 SQUID

A *SQUID* magnetometer is the most sensitive device to measure magnetic fields, although the signal is not detected directly from the sample. Detection coils are a single piece of superconducting wire, wound as a three coil set in a second-order gradiometer arrangement, shown in Fig. 3.2.

This configuration is composed of an upper coil with a single turn wound clockwise, the center coil has two turns wound counter-clockwise and a bottom coil similar to the upper one. Similarly to the *VSM* experiment, this coil configuration allows a background cancelling, by the counter-wounded outside coils, felt by the detection coil, while reading the magnetic

[8] source by: https://upload.wikimedia.org/wikipedia/commons/thumb/f/f2/VSM_en.svg/2000px-VSM_en.svg.png

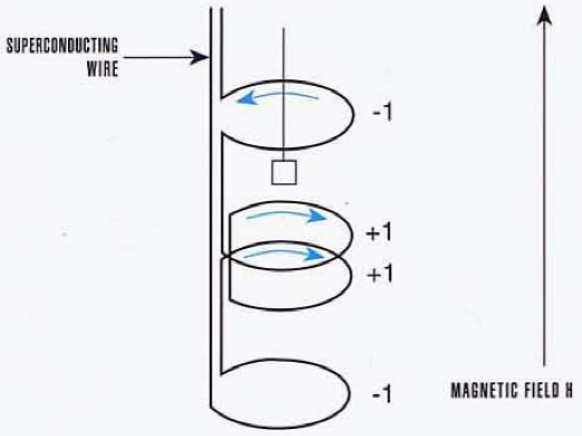

Fig. 3.2 Configuration of a second-order gradiometer used in *SQUID* equipments [8].

moment of the moving sample. As seen before, the magnetic moment of the sample can induce an electric current in the detection coil.

In the case of *SQUID* magnetometers, the measuring module is a closed loop of superconducting wire, so that a magnetic flux change in the detection coil produces a variation in the persistent current flowing through the circuit, feeding the signal to a superconductor coil that interfaces with the exterior measurement system.

A properly configured *SQUID* magnetometer electronics produces an output voltage exactly proportional to the current flowing through the detection coils to the *SQUID* input coil.

3.2 AC Magnetometry

Differently from DC magnetometry, in AC measurements the applied field is driven by a small AC current, causing a time dependent moment in the sample. This time dependence is able to induce an electric current in the pickup coil, allowing measurements of a static sample. [7]

In the limit of low frequencies, where a comparison with DC measurements is possible, the time dependent moment can be expressed by:

$$M_{ac} = \frac{dM}{dH} H_{ac} \cos(\omega t) \tag{3.2}$$

where H_{ac} is the amplitude of the applied field, ω is the driving frequency, and the susceptibility, χ, of the sample is represented by $\frac{dM}{dH}$ which is the slope of the $M(H)$ curve.

Because the susceptibility depends on the first derivative of the sample magnetic moment, the sensitivity of the instrument is very high for small changes in $M(H)$ and, since the

instrument depends on the slope of this curve, small magnetic shifts can be measured accurately even when the absolute moment of the sample is very large.

When the driving frequency increases, the similarity to DC magnetometry vanishes due to dynamic effects in the sample, reason why AC Susceptibility is also known as dynamic susceptibility. In this higher frequency regime, the magnetic moment of the sample is not able to follow the driving field and starts to lag behind. This effect is sensed by the detection circuitry ending in the measurement of two quantities: the magnitude of susceptibility, χ, and the phase shift due to the sample lag, ϕ, relative to the driving signal.

AC susceptibility has an in-phase component, χ', also known as real component, and an out-of-phase component, χ'', or imaginary component:

$$\chi = \chi' + i\chi'' \tag{3.3}$$

The magnitude and the phase shift are related to χ' and χ'' by the following relations:

$$\begin{aligned} \chi' &= \chi \cos\phi \\ \chi'' &= \chi \sin\phi \end{aligned} \quad \Leftrightarrow \quad \begin{aligned} \chi &= \sqrt{\chi'^2 + \chi''^2} \\ \phi &= \arctan\left(\frac{\chi''}{\chi'}\right) \end{aligned} \tag{3.4}$$

The imaginary component χ'' indicates dissipative processes occurring in the sample, that have different causes for each material measured. Also, both components of the dynamic susceptibility are sensitive to thermodynamic phase changes and this method can, with this characteristic, measure transition temperatures.

Different measurement processes access different information and the most used measurements are:

- χ vs. Temperature
- χ vs. Driving frequency
- χ vs. DC field bias
- χ vs. AC field amplitude
- Harmonic measurements

3.2.1 AC Susceptibility

In a more in-depth look at the magnetic response of the sample, when a varying field is applied, presuming $H_a = H_{a0}\cos\omega t$, the sample will present a phase lag.

Even when H_{a0} has a small amplitude, the response will be, in general, a non-linear signal in a distorted periodic wave. The distortion of the wave form can not be expressed as a sinusoidal function of single frequency, and for that reason the average of the local flux density must be described by a Fourier expansion [9],

$$\langle B \rangle = \mu_0 H_{a0} \sum_{n=1}^{\infty} \left[\mu_n' \cos(n\omega t) + \mu_n'' \sin(n\omega t) \right] \tag{3.5}$$

where μ_n' and μ_n'' are the real and imaginary components of relative permeability of μ_n, and n represents the frequency harmonics. Multiplying now both elements of the equation by $\cos(\omega t)$ and integrating over one period, from 0 to $\frac{2\pi}{\omega}$:

$$\int_0^{\frac{2\pi}{\omega}} \langle B \rangle \cos(\omega t)\, dt = \mu_0 H_{a0} \frac{\pi}{\omega} \mu_1' \tag{3.6}$$

and again multiplying now by $\sin(\omega t)$ we get:

$$\int_0^{\frac{2\pi}{\omega}} \langle B \rangle \sin(\omega t)\, dt = \mu_0 H_{a0} \frac{\pi}{\omega} \mu_1'' \tag{3.7}$$

As seen before, relative permeability and susceptibility are related by:

$$\mu = 1 + \chi, \tag{3.8}$$

And this relation applies to all harmonics on χ and μ. From now on we shall refer to χ_1' and μ_1' simply by χ' and μ' and similarly for the imaginary components.

Therefore:

$$\chi' = \mu' - 1 \tag{3.9}$$

$$\chi'' = \mu''. \tag{3.10}$$

From here one is now able to define both real and imaginary components of susceptibility in terms of $\langle B \rangle$:

$$\chi' = \left(\frac{\omega}{\pi \mu_0 H_{a0}} \int_0^{\frac{2\pi}{\omega}} \langle B \rangle \cos(\omega t) dt \right) - 1 \tag{3.11}$$

and

$$\chi'' = \left(\frac{\omega}{\pi \mu_0 H_{a0}} \int_0^{\frac{2\pi}{\omega}} \langle B \rangle \sin(\omega t) dt \right). \tag{3.12}$$

Expressed now, both components, in terms of the total magnetic flux, it becomes easier to understand what represents each one of them. χ' and χ'' are the quantities measured in an AC magnetometry experiment.

From Eq. 3.11, one can understand that χ' expresses the amount of magnetic flux penetration into the sample, for example, when the sample in study is a superconductor, χ' tends to -1, since this material, at low temperatures, behaves as a perfect diamagnet. The Meissner effect that occurs in this state prevents the magnetic field from entering the material, and thus $\chi' = -1$, meaning the permeability of the sample is $\mu' = 0$.

The imaginary component of susceptibility, χ'', is harder to grasp, since the information that can be taken from it depends on the analysed material and its behaviour. For some materials, the imaginary component, χ'' is nearly zero, meaning that, from Eq. 3.4, the magnetization will be perfectly in phase with the induced field if the material is paramagnetic ($\chi' > 0$) or out of phase if the material is diamagnetic ($\chi' < 0$).

Only positive values are physically possible for the imaginary component, meaning $\chi'' > 0$, and that can be seen from its relation with the power density given by the sample:

$$p = -M \frac{dB_a}{dt} \tag{3.13}$$

reaching an average value of:

$$p_{av} = \frac{1}{2} \mu_0 \omega H_0^2 \chi'' \tag{3.14}$$

over one complete cycle [14]. This value must be, obviously non-negative, thus $\chi'' > 0$.

3.2.2 AC Susceptometer

The susceptometer for AC measurements usually has a configuration with a primary coil coaxially wound over two secondary, pickup, coils wound in opposite directions and electrically connected in series.

The primary coil, or excitation coil, should produce a near-uniform ac magnetic field. As the pickup coils are wound in opposition, the total magnetic flux induced, without sample and from unwanted external sources, is ideally zero since one of the coils generates a current with same magnitude and opposite direction of the other one, meaning an equilibrium state is achieved.

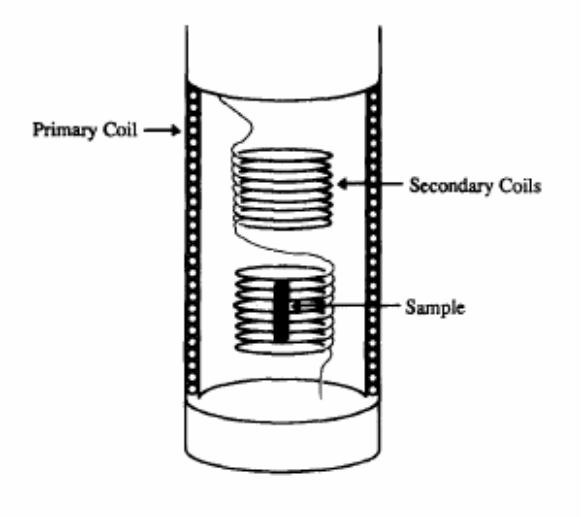

Fig. 3.3 Coil configuration of the AC Susceptometer [9].

When the sample is placed at the center of one of the pickup coils the equilibrium state will be broken and the measured rms voltage sensed across the secondary coils will be:

$$v(t) = -\frac{d\Phi}{dt} \tag{3.15}$$

which is related to the sample response and is dependent on time due to the AC field.

The magnetic flux induced by a sample with magnetization $M(H)$ in a pickup coil with N turns and a radius a results in[9]:

$$\Phi = \mu_0 \pi a^2 N M(t) \tag{3.16}$$

as the induced magnetic flux from the primary coil cancels:

$$\Phi = \mu_0 \pi a^2 N[(M + H_a) - H_a]. \tag{3.17}$$

Deriving now Eq. 3.16 according to Eq. 3.15 the measured voltage comes as:

$$v(t) = -\mu_0 \pi a^2 N \frac{dM(t)}{dt}. \tag{3.18}$$

To analyse the sample magnetization according to the time dependence, in terms of both components of susceptibility it is necessary to do a Fourier expansion just like in Eq. 3.5 for the local flux density:

$$M(t) = \sum_{n=1}^{\infty} H_{a0}(\chi_n' \cos(n\omega t) + \chi_n'' \sin(n\omega t)) \tag{3.19}$$

Replacing now the magnetization onto the measured voltage:

$$v(t) = \mu_0 \pi a^2 \omega N H_{a0} \sum_{n=1}^{\infty} n(\chi'_n \sin(n\omega t) + \chi''_n \cos(n\omega t)) \tag{3.20}$$

and taking $\mu_0 \pi a^2 \omega N H_{a0} = v_0$ using only the fundamental voltage, $n = 1$:

$$v(t) = v_0(\chi' \sin(\omega t) + \chi'' \cos(\omega t)) \tag{3.21}$$

This voltage is usually measured in synchronous phase locked loop with the excitation source, using a lock-in amplifier that enables to extract small signals from a possibly noisy background.

3.2.3 Phase Transitions

The sensitivity of AC Susceptibility coupled with the Lock-in Amplifier allows even small changes of the sample's susceptibility due to magnetic transitions. Typical cases are described below.

Superconductivity

Superconductivity is a magnetic state comprised of various physical unique properties, with the down side that it needs to be cooled bellow a transition temperature sometimes lower then the liquid nitrogen. At room temperature, the superconductor shows no particular effect, neither magnetic, nor electric.

When the superconductor is subjected to temperatures below the critical point, T_C, it behaves as a perfect diamagnet, which exposed to a DC magnetic field is able to expel all the magnetic field from its interior, because of superconducting currents shielding the whole sample due to the Meissner effect.

Perfect diamagnetism means that, when in this state, the superconductor has a negative susceptibility $\chi = -1$, reducing the magnetic flux to $B = 0$.

This property raises interest because it can be use for the calibration of an AC Susceptometer and determining if temperature readings on a cryogenic system are precise since this transition can be very sharp, like the one presented in Fig. 3.4.

When studying a superconductor, AC Susceptibility can determine its critical temperature, but has as well other advantage, over DC magnetometry. As previously referred, a DC field applied to a superconductor is totally expelled from its interior due to currents generated on

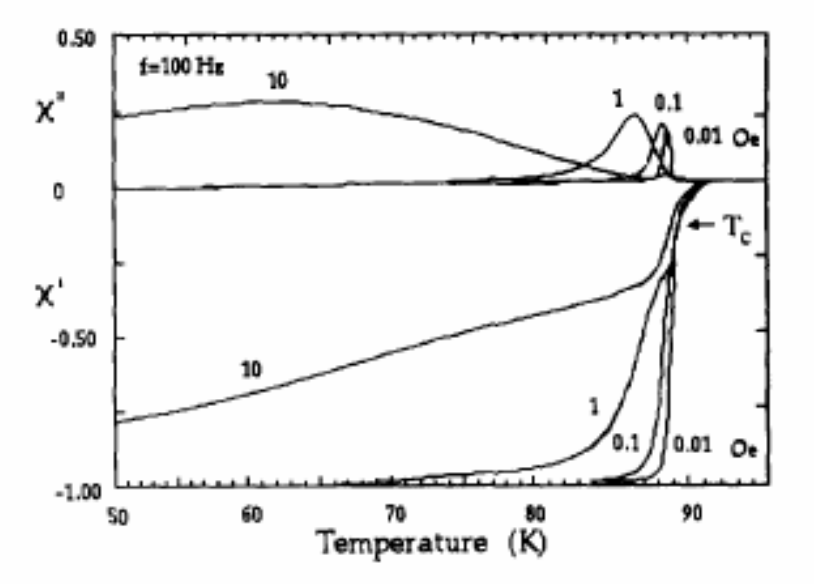

Fig. 3.4 AC Susceptibility of a superconductor sample [9].

the surface. For AC Susceptometry, the applied AC field can penetrate the sample surface, allowing measurements to determine important mechanisms of the flux dynamics.

From the imaginary component of susceptibility, one can determine other properties from superconductors, such as the critical current density.

Spin-Glass

These materials can be better explored by AC Susceptibility than other type of magnetometry. In a spin-glass system, magnetic spins feel random interactions with other magnetic spins and consequently form a metastable and highly irreversible state.

One important parameter in these systems is the freezing temperature, T_F which marks the transition from a paramagnetic state, at high temperatures, to a spin-glass state bellow T_F.

The importance of AC Susceptibility for measurements of this magnetic state is due to the frequency dependence of the curve χ' vs. T, near T_F. Another reason is that, being irreversible, this state provides a non-zero out-of-phase component, from where one can draw conclusions about the temperature treatment the sample was subjected to, due to the "memory" effects exhibited by spin-glass systems.

Magnetic Phase Transitions

Just like DC measurements, AC susceptibility is able to examine the nature of magnetic phase transitions at low frequencies.

Superparamagnetism

This theory was originally explained by Néel and Brown, characterizing small ferromagnetic particles that exhibited superparamagnetic properties. The transition temperature became known as the blocking temperature T_B and marked the temperature at which particles change for single-domain ferromagnetic behaviour ($< T_B$) to became superparamagnets ($> T_B$).

In the superparamagnetic state each particle's magnetic moment freely rotates, so a collection of particles acts like a paramagnet where the constituent moments are ferromagnetic particles.

AC Susceptibility takes a great role in these measurements because the behaviours of χ' and χ'' can provide additional information about particle interactions and the distribution of particle sizes. [7]

Chapter 4

Experimental Setup

As a whole, the system we implemented for AC susceptometry has a, rather simple, setup with a few key components that provide a good experimental environment. The system is briefly described in the following picture:

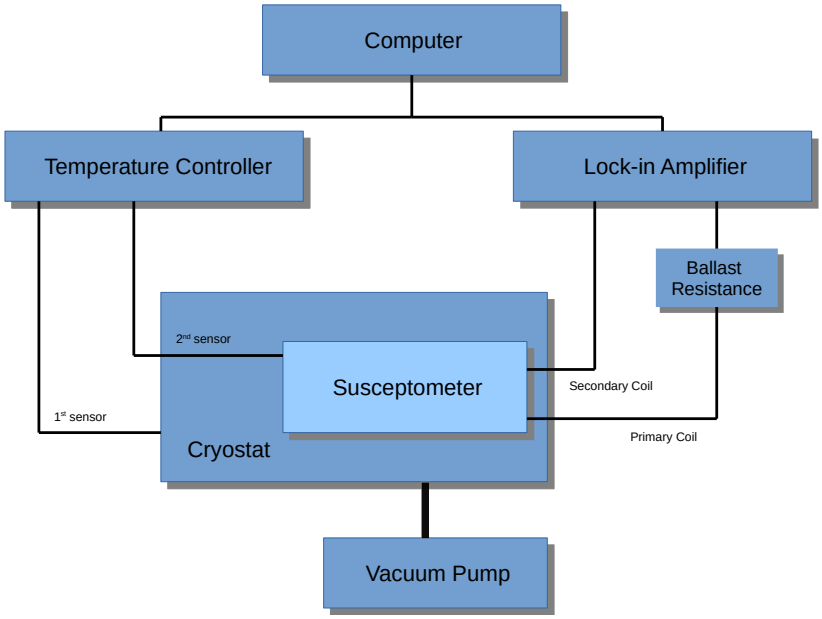

Fig. 4.1 System Set-up for the AC susteptometer.

4.1 Computer

The computer is used for the data acquisition and storage. The data is collected and processed using a Python program running under the Linux Operating System.

The connection from the computer to the Lock-in Amplifier is made by an RS232 Serial communication Port and to the Temperature Controller as USB communication with an internal RS232 converter.

The system fully exploits the possibility to work remotely with both the *LIA* and Temperature Controller meaning that, after developing drivers for the communication between machines, the computer was able to maintain the whole process with one main program managing all the tasks.

For all the programming work, as referred previously, Python was selected as the programming language as the interaction with the main operating system is so fluent and for the enormous community that provides support from forums and other communication platforms.

4.2 Lock-in Amplifier

For the susceptibility measurement we use an SR830 DSP Lock-In Amplifier (*LIA*) from Stanford Research Systems. This device meets two requirements of this system: provides a current source to feed the primary susceptometer coil as well as an input module able to sense the potential difference from the secondary coil and deliver it to the computer, after suitable filtering and amplification.

The Lock-in and the phase sensitive detection (*PSD*) will be discussed in more depth in chapter 5 considering the elaborate process attached to it.

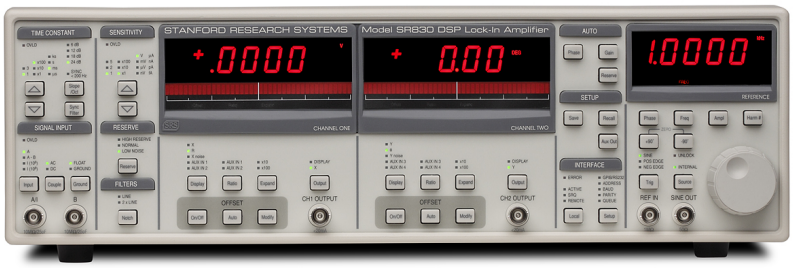

Fig. 4.2 Front end of the Lock-in Amplifier. [9]

As for the excitation of the primary coil, the *LIA* requires a reference oscillator phase-locked to the signal frequency. This can be accomplished by an internal oscillator or by a external reference signal, higher than 200 mV pk, that is provided to an AC coupled input (above 1 Hz) with an impedance of 1 MΩ.

[9] source by: http://www.thinksrs.com/assets/instr/SR810830/SR830_FPlg.jpg

The external reference signal can trigger with either an analogic signal or a TTL signal, considering the zero of the reference phase shift the positive zero crossing or edge. Using this mode, the internal sine wave is phase-locked to the external reference. [12]

When the external reference doesn't exist, the phase-locked-loop is not used, and the output sine wave provides the excitation to the experiment. In this situation the phase shift is user selected or remotely defined.

The output excitation signal is digitally synthesized by a digital signal processor (*DSP*) with a 16-bit *DAC*, sampling at 256 kHz, aided by an anti-aliasing filter converting the generated signal to a low distortion sine wave. The output wave amplitude can vary from 4 mV to 5 V and has a frequency range limit at 100 kHz.

4.3 Ballaster Resistence

The ballaster resistance is placed in series with the *LIA* output and the primary coil of the susceptometer, serving as a current limiter for some experiments, when needed.

In the case there is a current source, the ballaster resistance can be used as the voltage drop reference for the *LIA*, and is still used in series with the primary coil of the susceptometer. For some cases, the function generator provides a $TTL\ SYNC$ output which can replace the ballaster resistance.

4.4 Susceptometer

For these experiments the susceptometer used was wounded in a perspex tube with a length of 2,5 cm and a 5 mm radius.

Unlike the usual susceptometer, where the primary coil is wound over the secondary coils, for the project the configuration was the opposite. The primary coil was wounded first over the perspex tube with 600 turns and the secondary was wound over that with the same number of turns in each coil, presented in Fig. 4.3.

Due to an irregular shape and a low thermal contact between the susceptometer and the sample holder, an aluminium foil was used, as a gasket material, in order to increase thermal contact, easily adapting to the rough surface and decreasing the thermal lag from on point to the other.

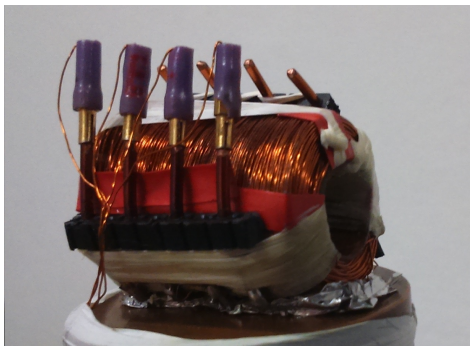

Fig. 4.3 AC Susceptometer coils.

4.5 Cryostat

The whole cryostat is an ensemble of four different components: Vacuum Pump, Temperature Controller, Compressor and Expander. All these are connected like shown schematically in Fig. 4.7.

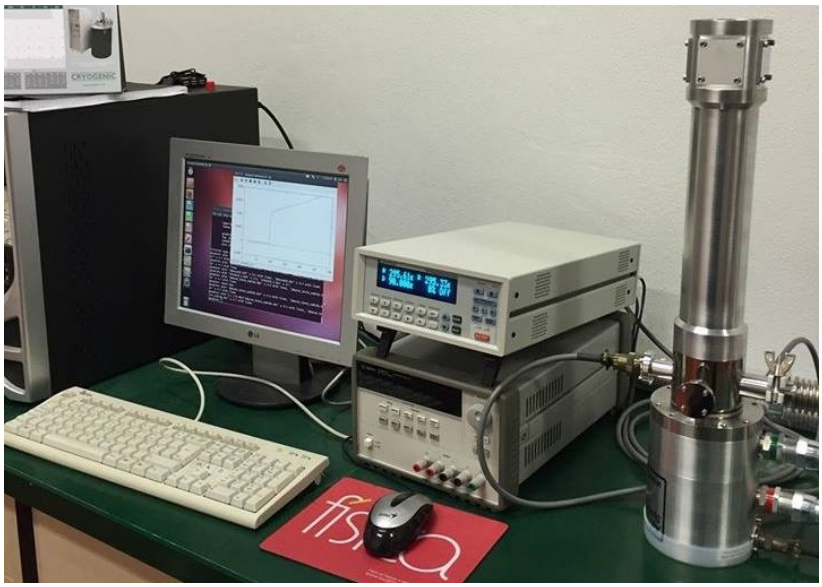

Fig. 4.4 Workspace with cryostat, temperature controller and computer.

4.5.1 Compressor

The cryostat relies on a water cooled Helium compressor for the flow of pressurized helium to be supplied to the expander, where the cooling happens.

The expander is linked to the compressor by two gas flow lines and an electrical power cable. The gas flow lines supply high pressured helium, while the other one returns the low

pressure helium to the compressor. The power supply is used to drive a motor which turns a valve disc inside the expander.

4.5.2 Expander

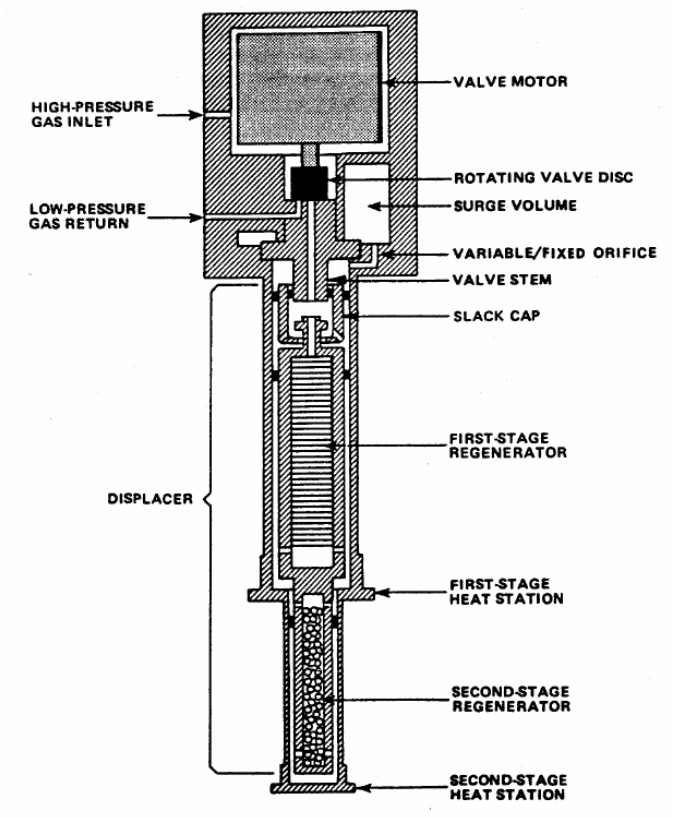

Fig. 4.5 Diagram of the expander with a two stage GM refrigerator. [10]

The cooling power is provided by the expander, that operates on the principle of a Gifford-McMahon (GM) refrigerator cycle, and that means a gas compression-expansion cycle. This process begins with the compression of the gas, whose work done is then rejected to the system surroundings, and the cooling is produced in a separate chamber when the expansion of the gas takes place.

GM refrigerators

A GM refrigerator can be found in use in many applications because it is a robust system that can be used for many widespread applications. This kind of refrigerators can easily cool

[10] source by: http://www.coldedgetech.com/uploads/files/257519A%20DE-202%20DE-204%20DE-208R%20DE-208L%20Operating%20Manual.pdf

from room temperature to temperatures below 10 K, filling a wide range of purposes without much effort.

One advantage of the GM refrigerators is the uncoupling of the compressor that works at powerline frequency, from the expander who works at much lower frequencies (sometimes less than 1 Hz). But, this system as a great disadvantage. The valve cycles are made of irreversible processes, that means the whole cycle must be as efficient as possible.

Efficiency is improved by the use of regenerators that keep heat stored for a short time, so in the next cycle of the refrigerator the heat output can be reinserted again in the cooling process.

- **From a to b:** The supply (high pressure) line is connected to the valve and the expander's displacer moves to the left, forcing the gas to go through the regenerator. At this point, the gas that entered the system cooled to the same temperature as the regenerator.
- **From b to c:** The cooling takes place when the return line is connected and the gas starts to expand, where an isothermal expansion takes the heat from the cold space.
- **From c to d:** With the return (low pressure) line still connected, the displacer moves to the right forcing the cold gas to pass through the regenerator and returning it to the compressor.
- **From d to a:** The rotatory valve reconnects the supply line and restarts the cycle.

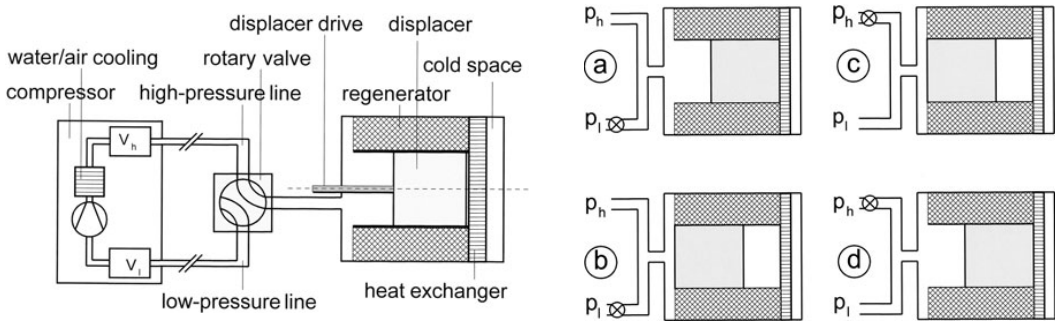

(a) Schematic diagram of a GM-cooler

(b) The four stages of the GM cooler

Fig. 4.6 Gifford-McMahon refrigerator diagram and stages [2].

A cycle of this cooler can be split in four stages [13], presented in Fig. 4.6b. [2]

Expander Stages

As shown in Fig. 4.5 and in Fig. 4.7, the expander has two stages, both with a respective regenerator and heat station, with different functions and different cooling powers.

First of all, exists a vacuum shroud that covers all the cold section of the expander. As said before, vacuum is the best thermal insulator and prevents heat exchange with the exterior.

Attached to the first stage heat station is placed the radiation shield. In this system an actively cooled radiation shield is used, and can drop below 40 K, reducing heating transferred from the environment in the form of radiation, such as infrared radiation.

In the second stage it is mounted a sample holder with a indium gasket to improve thermal conductivity. This stage can reach temperatures below 10 K.

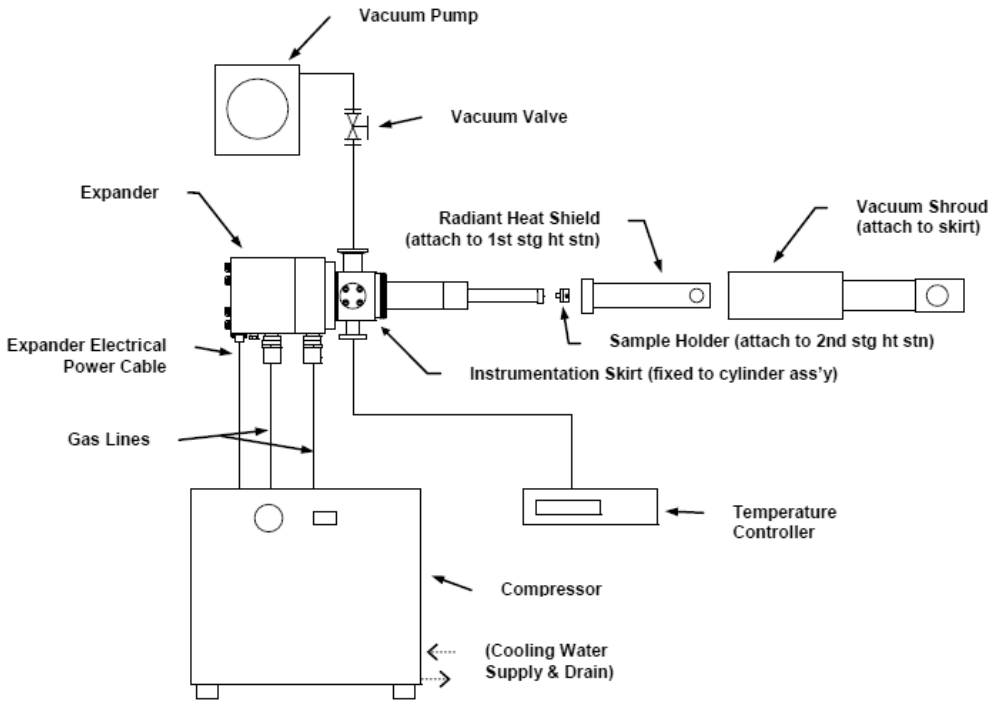

Fig. 4.7 Complete diagram of the cryostat system with simple shroud, radiation shield and sample holder.

4.6 Vacuum Pump

Vacuum is the best thermal insulator, and for that reason, the system uses a TPS-Compact Vacuum Pump able to reach high vacuum levels with a turbomolecular pump.

In the first stage of the vacuum, a primary scroll pump is activated to achieve an adequate vacuum level before activating the turbopump. This scroll pump is composed of two different scrolls, one is fixed and the second orbits the first, creating zones of captured gas, which is posteriorly displaced, compressed and exhausted.

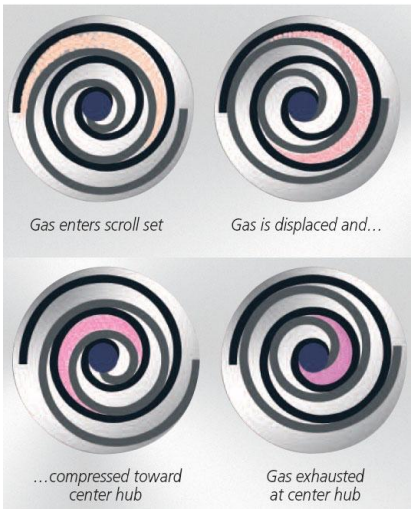

(a) Scroll Pump function diagram [1].

(b) A cutaway view of a turbomolecular high vacuum pump.[11]

Fig. 4.8 Primary and Turbomolecular pumps of a High Vacuum Pump.

The turbopump is a high frequency motor driving turbine equipped with many bladed stages and Macrotorr stages. This turbine is made of high-strength, light aluminium alloy, made from a single block of the alloy. The turbine blades have five different angles, from 44° to 12°, while the Macrotorr stages are in the form of discs.

The turbine rotor is supported by permanently lubricated high precision ceramic ball bearings installed on the forevacuum side of the pump. The static blades of the stator are fabricated in stainless steel. These are supported and accurately positioned by spacer rings.

The Macrotorr stators are in the form of selfpositioning machined discs with pumping channels and an opening restricted by the corresponding rotor discs which are fabricated in aluminium alloy. [1]

[11] source by: https://upload.wikimedia.org/wikipedia/commons/4/4c/Cut_through_turbomolecular_pump.jpg

4.7 Temperature Controller

For the control of the cryostat temperature, we use a LakeShore Model 335 Temperature Controller, which is a two-channel temperature controller with user configurable heater outputs that deliver a total of 75 W of low noise heater power. [5]

This controller is easy to use due to the intrinsic control functions, such as ramps, PID control, standard interface and a series of simple commands that provided an easy way to develop a useful driver.

4.7.1 Temperature Sensors

Temperature sensors are a sensitive component of temperature control, and should be properly selected taking into account the expected span of temperatures and the required accuracy and precision. Cases exist when a temperature range is much wider then one sensor useful range and setups with two different sensors that complement each other and tightly cover the whole range of temperatures may be required.

As our experiments are preformed from 8 K to room temperature, the simple Si diode sensor close to the sample and another similar sensor close to the cryostat base are enough for temperature control.

Other important aspect of the temperature measurement is the location of the sensors , that might be a difficult feat in crowded cryostats. For that reason, one issue that can lead to wrong temperature readings are the temperature gradients that happen in any system because there rarely exists a perfect balance between cooling and heating source. For better readings, the sensor must be near the sample, so both are affected equally.

4.7.2 Heater

The heater works as the controlled heat source of the system, and needs to provide enough heat power to warm the system so it can work in the design temperature ranges.

The heater should as well be chosen according to the task and the shape of the cold tip, so, for this experiment, there is a foil heater to provide the control. This type of heater is composed of a thin layer of resistive material adhered to electrically insulating sheets, as shown in Fig. 4.9.

This heater should be of proper size for each set-up, so it can be in good thermal contact with the active area, not only for a maximum benefit of the heating power, but to keep spots in the heater from over heating and burning out. The high vacuum achieved for the experiments is a good thermal insulator, and can be an issue for the heater if the thermal contact with the

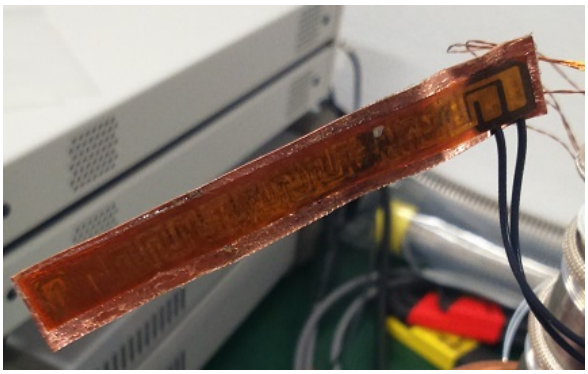

Fig. 4.9 Foil heater glued to a cooper foil

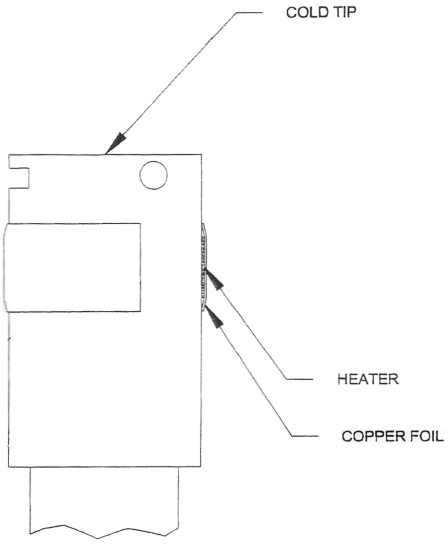

(a) Foil heater diagram without Kapton

(b) Cold tip and foil heater with Kapton cover

Fig. 4.10 Foil Heater and diagram of application to the cold tip

cold tip is feeble. To achieve a better and viable contact, a Kapton shrink tape is wrapped around the heater so it can tightly press the heater and the copper foil against the cold tip, as showed in Fig. 4.10.

Thermal anchoring should be used for the wires that drive the current to the heater, so they don't overheat, fuse and ruin the temperature control.

The location of the heater should be in close thermal contact with the cooling power, so it can provide a better measurement accuracy, control and minimize the temperature gradient.

Other cautions must be considered so the heater may be preserved, such as, a method to limit the current, since the output for the heater is a current source, and that can be done by

using low ramps or fitting the source to the heater used. The Model 335 as inherent functions that can be set to accomplish that.

4.7.3 Control Optimization

Besides the techniques already discussed for each part of the temperature control, there are other tips to achieve optimum temperature control, described bellow.

Thermal Conductivity

Thermal conductivity is an important characteristic of materials that should be kept in mind. The use of materials with good thermal conductivity is assured in the cryostat, but can be improved in the components added to the system. The first thing to attend to are the junctions of the control loop, they must be in close thermal contact, and that can be accomplished with a gasket material, such as indium, or cryogenic greases that can increase the effective contact area.

Gasket materials should be applied in rough mating surfaces to increase the contact area, like sensors or sample holders, these materials should always be used with reasonable pressure, good gasket material are soft, thin and have good thermal conductivity.

Cryogenic greases can be used to different shaped surfaces, such as sample and sample holder providing a better thermal equilibrium between those components with the increase contact area.

All these materials should be able to withstand rough conditions because they are subjected to high vacuum pressure and cryogenic temperatures.

Thermal Mass

For a good thermal control, something very important to consider is the thermal mass of the system. The cryostat is packed big components and, the more mass that is added to the system, the harder it is to cool everything. The cooling process will be slower and the base temperature will be higher, nothing needed in a cryogenic system.

One more problem that arises with a high thermal mass, as well as poor thermal contact, is temperature gradients that make equilibrium and control an even harder task.

Low thermal mass can also be problematic. In this situation there is no buffer to absorb small temperature changes, and small disturbances can cause a large variation in temperature measurements and stability becomes poorer.

Two-Sensor Approach

Although there are many complications and setbacks in temperature control and measurement, in systems that is difficult to set an optimal location for one sensor to accomplish both tasks, a two-sensor approach is used.

For this reason, there are two sensors in our system, that meet different objectives. The most common sensor is the one near the sample, and it provides clean and accurate measurements of the sample temperature. This sensor is subjected to the same conditions as the sample, including temperature gradients.

The other sensor is set to a location where the control of the system is easier, the feedback sensor, and that is near the cooling and heating source, where the thermal lag is minor.

4.7.4 PID Control

Working with a closed-loop operation, the temperature controller uses a *PID* control algorithm that regulates the heater output in order to soften the temperature warming and cooling curve.

The PID stands for proportional, integral and derivative, and controls the heater output implementing the following equation:

$$Heater\ Output = P\left[e\ +\ I\int(e)\,dt\ +\ D\,\frac{de}{dt}\right] \tag{4.1}$$

where error (e) is defined as: e = setpoint - feedback reading.

The values for this control loop depend on the system implemented because it is dependent on the load present on the cryostat. For our system the PID values after adjustments resulted in:

P	200
I	100
D	0

Table 4.1 PID control loop settings.

Proportional

Also called gain, the proportional term is multiplied by the error (e) to create its contribution to the output:

$$Output(P) = P\ e \tag{4.2}$$

This term alone, without using any other term, must always generate an error or the output will go to zero. This term is linked to the load of the system, as well as the sensors and the controlling system. The proportional setting is commonly determined by trial and error, as seen in Fig. 4.11 from *a*) to *c*).

Integral

The integral term is also known as reset and takes into consideration the error over time for its contribution to the output:

$$Output(I) = P\,I \int (e)\,dt \tag{4.3}$$

This term, added to the proportional contribution, can eliminate the necessary error from the proportional-only system as seen in Fig.4.11 d). When the error reaches zero, the output is maintained constant by the presence of the integral term. This term is related to the dominant time constant of the load, which means it is more predictable than the gain.

Derivative

And last is the derivative, also known as rate, which acts on the change in the error with time:

$$Output(D) = P\,D\,\frac{de}{dt} \tag{4.4}$$

Just like the integral term, the derivative is related to the dominant time constant of the load and is set relative to the integral contribution.

The derivative term can react to fast changing error signals by pushing the output signal, meaning it takes less time for the system to reach the setpoint and that it can reduce the output quickly so it decreases overshot.

Although it seems useful for a fast changing systems, the derivative term is usually turned off during steady state control, because of its fast and strong reaction to small changes that can cause temperature disturbances. As our system was based on slow temperature ramps this was the opted way to deal with the Integral term.

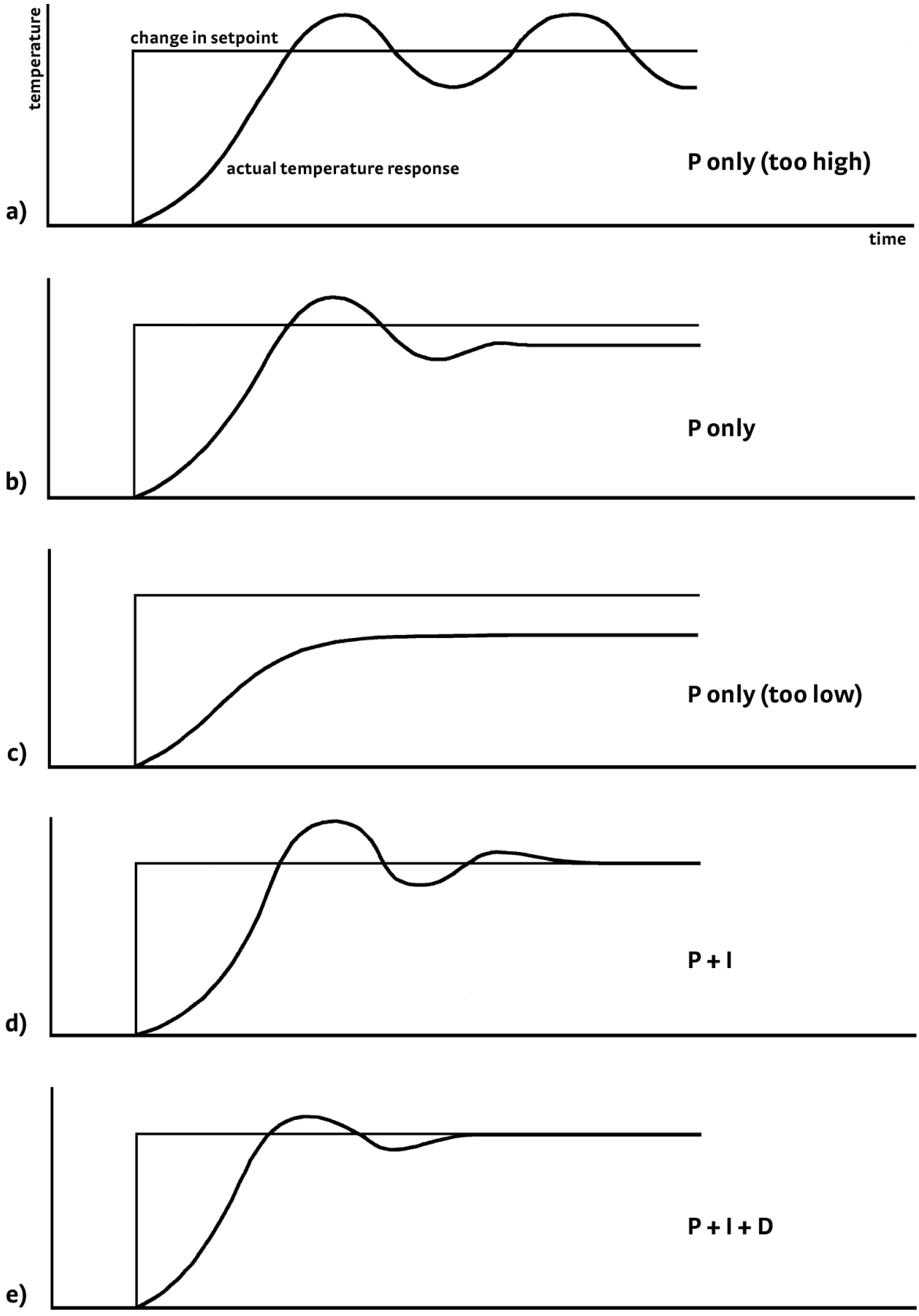

Fig. 4.11 Setting of the PID control loop steps[5].

Chapter 5

Lock-in Amplifier

The *LIA* works as a highly sensitive discriminating voltmeter which measures the amplitude and relative phase shift of the AC signal that the sample induces in the pickup coils. Although the measured signal is AC, the output of this equipment are DC values proportional to the characteristics of the probed signal.

This equipment is very useful in AC Susceptibility measurements due to its ability to isolate each of the components, real and imaginary. The high input impedance of the *LIA* allows measurements of the signal without the need to correct the thermal difference of the pickup coil since the input impedance is considerably higher than the coil's.

When measuring, one important concept, already discussed, is the fact that the values of χ'' must always be positive. If that isn't true, the signal must be wrong and needs just to be corrected or, the phase shift might not be correctly defined, mixing both components. For that, a phase correction is needed, although not very easy and straight forward, where both voltage signals are separated, correcting the phase:

$$v' = v_0 \cos\Theta + v_{90} \sin\Theta \tag{5.1}$$

$$v'' = v_{90} \cos\Theta - v_0 \sin\Theta \tag{5.2}$$

where v_0 and v_{90} are the *LIA* voltages at 0^o and at 90^o, v' is the in-phase voltage (Θ) and v'' is the out-of-phase voltage ($\Theta + 90^o$).

5.1 Phase Sensitive Detection

Measurements with this apparatus requires a frequency reference equal to the frequency of the driving AC field. With a fixed frequency in an experiment, the *LIA* is able to detect the response of the material at said frequency.

The sensed signal amounts to $V_{sig}\sin(\omega t + \theta_{sig})$, where V_{sig} is the signal amplitude while the internal reference will be a sine wave created by the lock-in, with the form of $V_L\sin(\omega_r t + \theta ref)$.

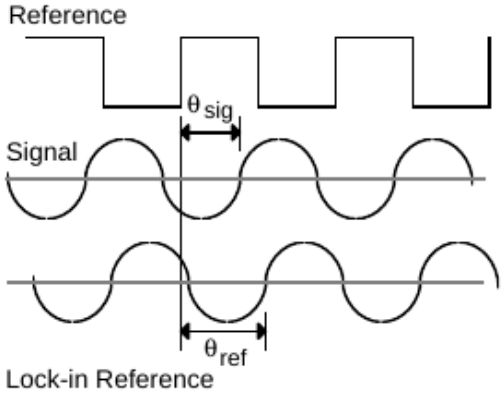

Fig. 5.1 Basic representation of the *PSD* reference signals[12].

The *LIA* will then amplify the signal and the phase sensitive detector will multiply them both, generating an output like:

$$V_{psd} = V_{sig}V_L\sin(\omega_r t + \theta_{sig})\sin(\omega_L t + \theta_{ref}) \tag{5.3}$$

$$= \frac{1}{2}V_{sig}V_L\cos([\omega_r - \omega_L]t + \theta_{sig} - \theta_{ref}) - \tag{5.4}$$

$$\frac{1}{2}V_{sig}V_L\cos([\omega_r + \omega_L]t + \theta_{sig} + \theta_{ref}) \tag{5.5}$$

that arrives to a solution with two signals, one from $(\omega_r - \omega_L)$ and another from $(\omega_r + \omega_L)$. [12]

Applying now the property of the *LIA* that both frequencies, from the signal and from the lock-in reference, are equal $(\omega_r = \omega_L)$, the difference from Eq. 5.3 becomes:

$$V_{psd} = \frac{1}{2}V_{sig}V_L\cos(\theta_{sig} - \theta_{ref}), \tag{5.6}$$

originating a voltage signal proportional to the amplitude.

5.1.1 Narrow Band Detection

The *LIA* is a suitable instrument for this kind of experiments since its detection is so sensitive and can nullify noise signals that use frequencies other than the one used by the experiment.

This is a really good feature since the *LIA* is able to detect a signal with frequency of 10 kHz with a bandwidth as narrow as 0.01 Hz.

5.1.2 Lock-in Reference

In *LIA* measurements it is need a reference signal, and not only that, the reference has to be similar to the signal frequency, and that means the *LIA* as to be phase-locked to the reference for the *PSD* to work properly.

The reference signal, in *LIA* is produced with the use of a phase-locked-loop, that can easily lock the internal oscillator to the external reference signal, producing a sine wave with frequency ω_r and a phase shift θ_{ref}.

5.1.3 Magnitude and Phase

Recalling the *PSD* output, one can use the reference phase shift as the zero mark and with that:

$$V_{psd} = \frac{1}{2} V_{sig} V_L \cos(\theta_{sig}). \tag{5.7}$$

This result is only due to one *PSD*, usually Lock-in Amplifiers have generally two phase sensitive detectors. The first, as seen, measures the signal in phase with the reference source, while the second *PSD* multiplies the signal with a reference that is shifted 90^o ($V_L \sin(\omega_L t + \theta_{ref} + 90^o)$) and, after the low-pass filter, come as:

$$V_{psd2} = \frac{1}{2} V_{sig} V_L \sin(\theta_{sig}). \tag{5.8}$$

$$V_{psd2} \sim V_{sig} \sin(\theta_{sig}). \tag{5.9}$$

The output given by the *LIA* are called X and Y for the first and second *PSD* signal, respectively.

$$X = V_{sig} \cos(\theta) \tag{5.10}$$

$$Y = V_{sig} \sin(\theta) \tag{5.11}$$

The *LIA* can, as well, provide the values of magnitude, R, and phase shift,θ, computing:

$$R = (X^2 + Y^2)^{\frac{1}{2}} = V_{sig} \tag{5.12}$$

$$\theta = \arctan\left(\frac{Y}{X}\right) \tag{5.13}$$

Chapter 6

Results

During the test phase of our AC susceptometer, the behaviour of the coils and their the phase shift due to the temperature dependence of the wire resistance was investigated. Along with the phase shift, the values for the scale factor were determined from several runs.

After these calibrations, AC measurements of background (empty coils) and several samples were performed.

6.1 Phase Adjustment

In an ideal AC susceptometer, a current source is used so the applied field has the same amplitude throughout the experiment. In our case we replaced the current source by a voltage source through a ballast resistor that acted as a voltage divider and current limiter. In this case the adjustment of the phase is necessary so that the signal from the secondary coils is in the proper phase when read in the Lock-in Amplifier, compared to the ideal situation.

The expected phase shift, ϕ, from and ideal coil would be described by:

$$\phi = -\arctan\left(\frac{\omega L}{R}\right) - \phi_0, \tag{6.1}$$

where L is the coil inductance, R the resistance, and $\omega = 2\pi f$, where f is the frequency and $\phi_0 = -90^o$ the low frequency limit of the phase shift in the pick-up coils.

To ascertain the coil behaviour, the resistance and impedance where measured in various applied frequencies, as shown in Table 6.1.

The above equation does not reproduce well the measured phase shift for frequencies higher then 10 kHz due to several instrument effects. Therefore, an empirical formula $\phi(f)$ was fitted to the data as shown in Fig. 6.1.

f (Hz)	R (Ω)	L (mH)
50	33.790	5.760
100	33.854	5.234
1000	34.114	5.303
10000	35.663	5.289

Table 6.1 Values of resistance and inductance of primary coil, measured at various frequencies.

This empirical formula reproduces well the phase of the system except for a small region, between 18 kHz and 28 kHz corresponding to the coil resonance and it is a non-operating zone.

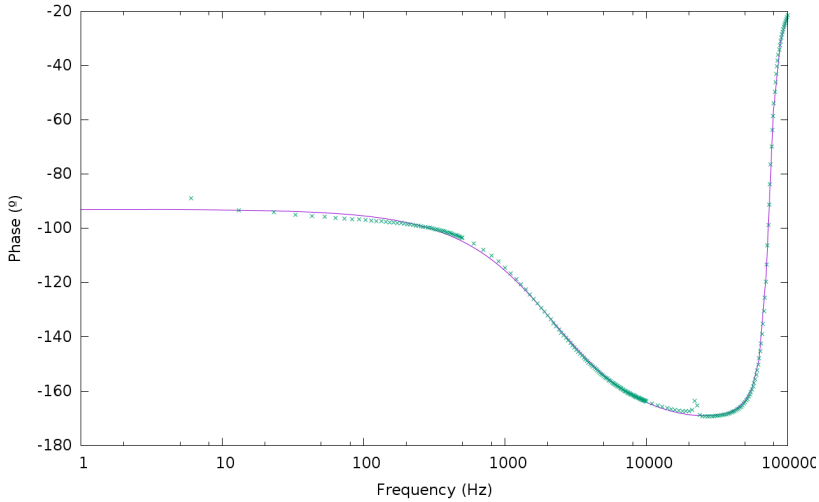

Fig. 6.1 Phase adjustment obtained from the dependance with frequency.

The phase shift is temperature dependent due to the change in wire resistance and dimensions of the coils. Therefore the phase shift was adjusted from several measurements at different temperatures. In Fig. 6.2 the phase shift is compared at 10 K and 300K. They present a similar behaviour for lower frequencies but, at higher frequencies, the phases starts to differ significantly, and that is a problem for measurements at high frequencies.

In Fig. 6.3 we show the scale factors as function of frequency determined from the observed offset values of the voltage.

6.2 Background adjustment

The background measurements were performed in order to correct the signal due to the expected changes in the primary coil field with temperature. These backgrounds were

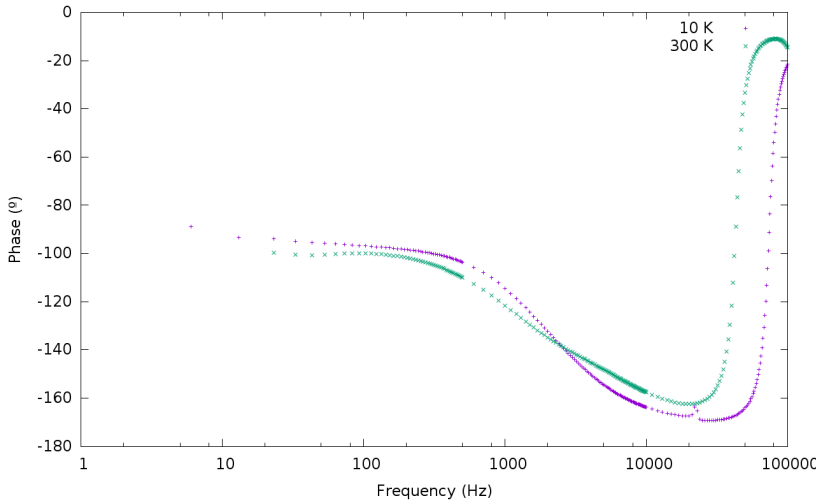

Fig. 6.2 Comparison of the phase shift at 10 and 300 K.

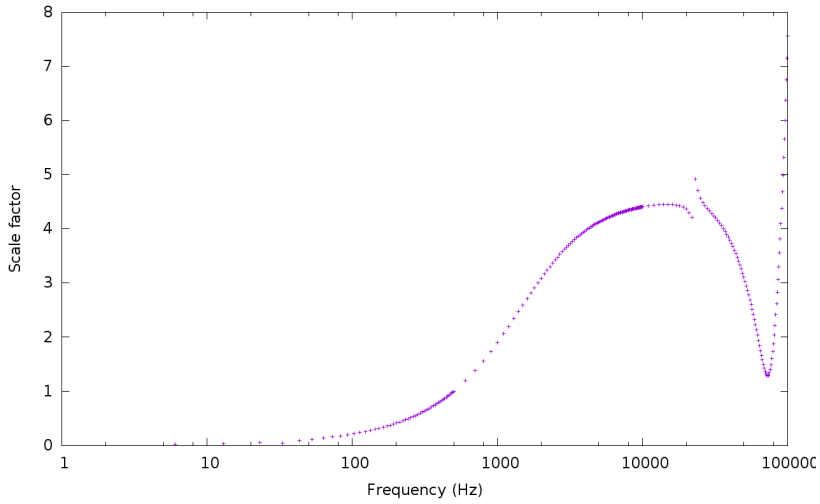

Fig. 6.3 Scale factor dependance with frequency.

subtracted from the data measured with samples. In order for the background subtraction to be valid, one should ensure that both background and sample data are measured with the same temperature rate. Temperature gradients in the coils affect somehow the background curves and these should therefore be minimized.

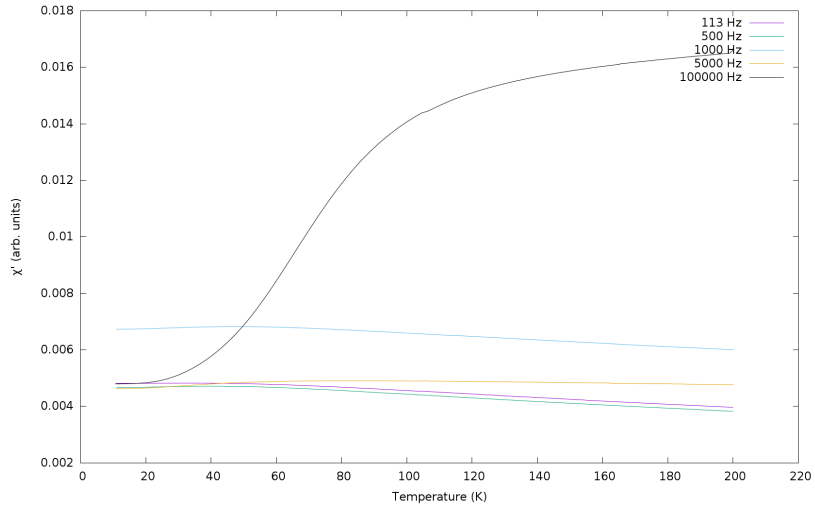

Fig. 6.4 Background signal from real component with temperature for different frequencies.

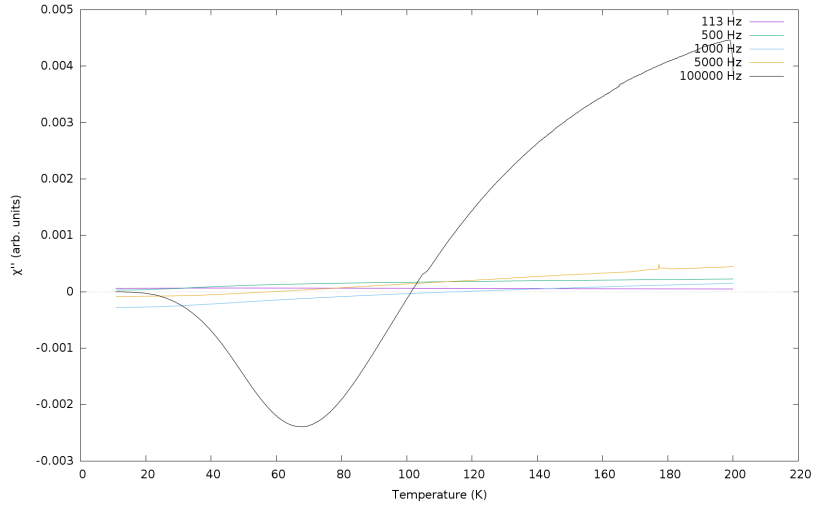

Fig. 6.5 Background signal from imaginary component with temperature for different frequencies.

6.3 Samples

The analysed samples were bulk YBaCuO and UFe_4Al_8, due to their sharp and characteristic transitions, both subjected to DC and AC measurements in order to validate temperature readings.

As for DC measurements, the employed method was the Vibrating Sample Magnetometer. The *VSM* system used was a PPMS® DynaCool™ (Physical Property Measurement System) from Quantum Design. We have performed both *ZFC* and *FC* measurements, which stand for Zero Field Cooling and Field Cooling.

In a ZFC experiment a sample is cooled without any magnetic field. When the desired low temperature is set, the warm up process starts with the presence of field and the measurements are acquired. After the maximum temperature is reached, the sample is cooled again, but now in the presence of the same field applied while the temperature increased (FC curve).

Since AC susceptometers measure the derivative of the sample magnetization and this is a difficult value to calibrate, most AC experiments are used to examine phase transitions in samples and its dependence with the magnetic field amplitude or frequency. For this reason, DC measurements were used to ascertain the transition temperature in both systems and to compare the information obtained from each method. AC susceptibility results for each sample were confirmed from bibliographic references.

6.3.1 YBaCuO

Bulk YBaCuO, as a superconductor, shows a transition, the so called Critial Temperature, T_C, at approximately 93 K when the sample behaves as a perfect diamagnet and shows a real susceptibility of $\chi' = -1$. It is a good start point for the instruments calibration since the susceptibility in both phases, superconductor and normal, paramagnetic phase, have very clear values, of $\chi' = -1$ and $\chi' = 0$, respectively.

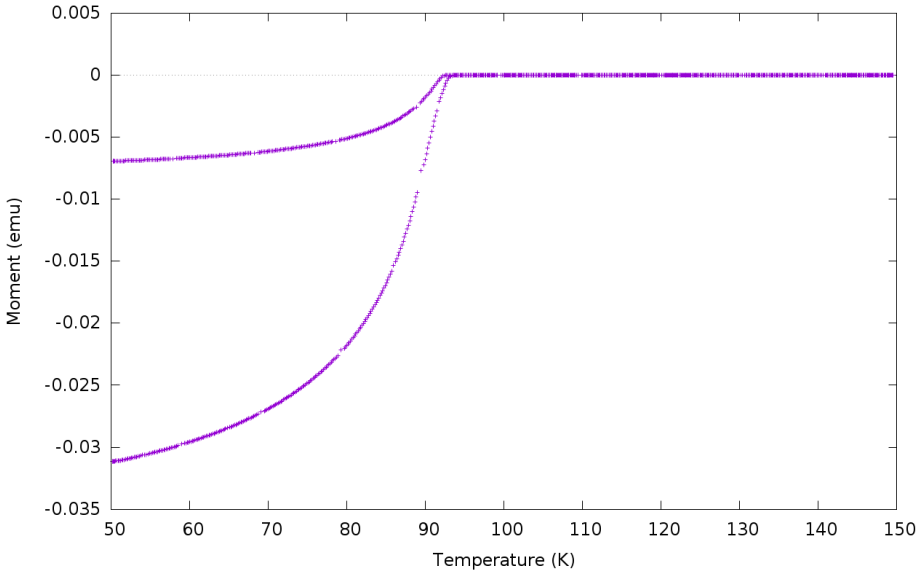

Fig. 6.6 ZFC and FC measurements of the YBaCuO sample.

In the *VSM* measurements, both in the *ZFC* as in the *FC*, the moment of the sample clearly tends to a negative value, as expected from a superconductor, presented in Fig. 6.6.

In the AC measurements, the sample as shown a transition at 95K, not far from the expected value, and a magnetic moment that increases with the frequency of the applied field, as shown in Fig. 6.7.

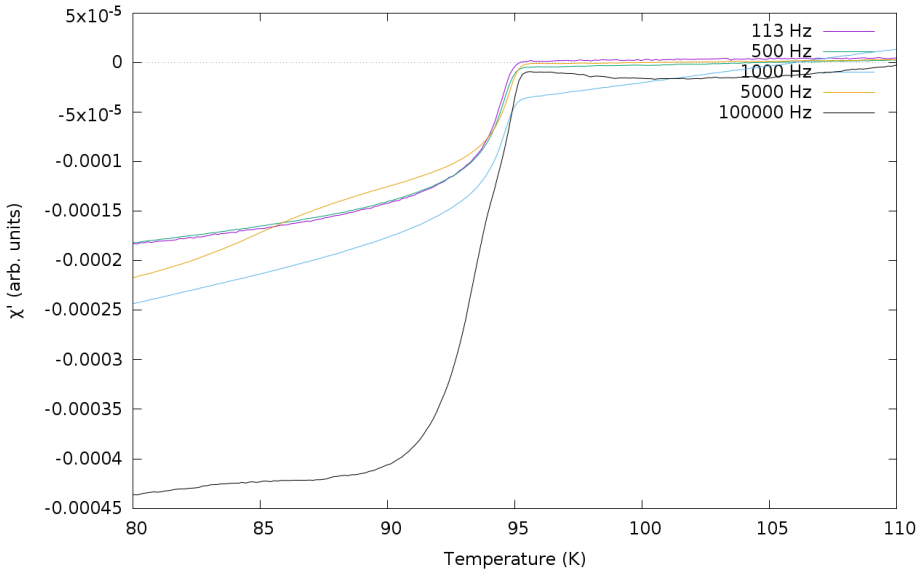

Fig. 6.7 Real component of YBaCuO's AC susceptibility. Data is shown for frequencies up to 100 kHz. The superconducting transition is clearly shown at 93K; below that temperature a strong diamagnetic signal (Meissner effect) is observed.

For the imaginary component of YBaCuO's susceptibility there is still a bit of tunning to perform to our system so that the results can reliably be used to interpret the real events in the sample. The imaginary component is particularly prone to systematic errors such as those arising from the phase of the primary coil during thermal cycling. As a consequence of the resistance changes, those phase shifts obviously affect the reference of the lock-in that is taken, to fix the phase, at a single temperature, as expected from the results obtained in Section 6.1.

In other words, the imaginary component is very sensitive to small shifts of the phase, that can be either due to the sample or to the thermal changes of the characteristics of the coil and it is difficult to disentangle them. In any case, the shape of $\chi''(T)$ curve with a small positive peak at T_C is expected for such compounds. All the results are shown in Fig. 6.8.

6.3.2 UFe_4Al_8

This sample is ferromagnetic with the Fe moments showing weak ferromagnetism and the U atoms carrying a ferrimagnetic component; this compound has been studied in detail by Paixão et al[10]. The sample we have used is a deuterated sample for which the single

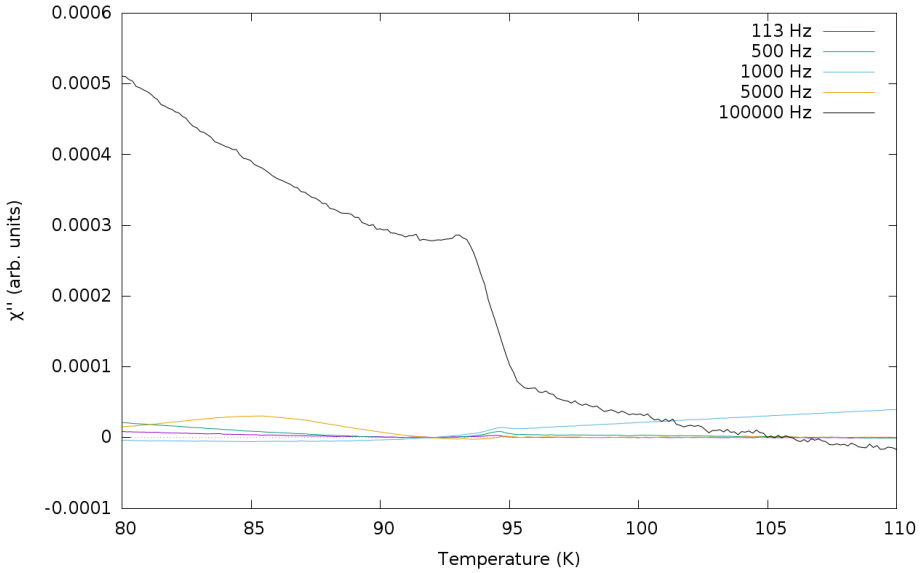

Fig. 6.8 Imaginary component of YBaCuO's AC susceptibility at different frequencies up to 100 kHz. At low frequencies an expected small positive signal is observed, representative of dissipative processes. The curve at 100 kHz is distinct and not reliable due to the wide variation of the phase shift with temperature in high frequency regime.

transition at T_C ($\sim$ 150 K) has developed into two close transitions, as inferred from other measurements.

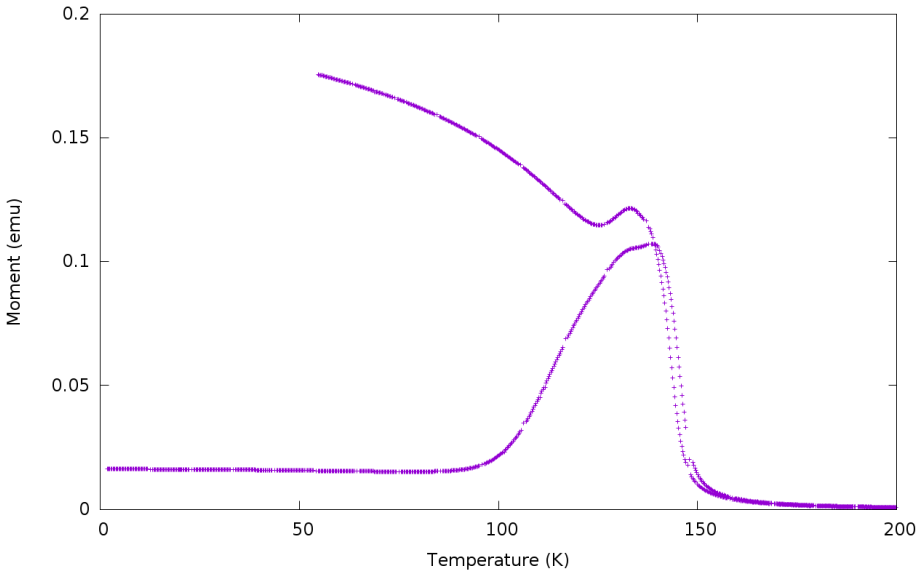

Fig. 6.9 ZFC and FC measurements of the UFe_4Al_8 sample with a field of 50 Oe.

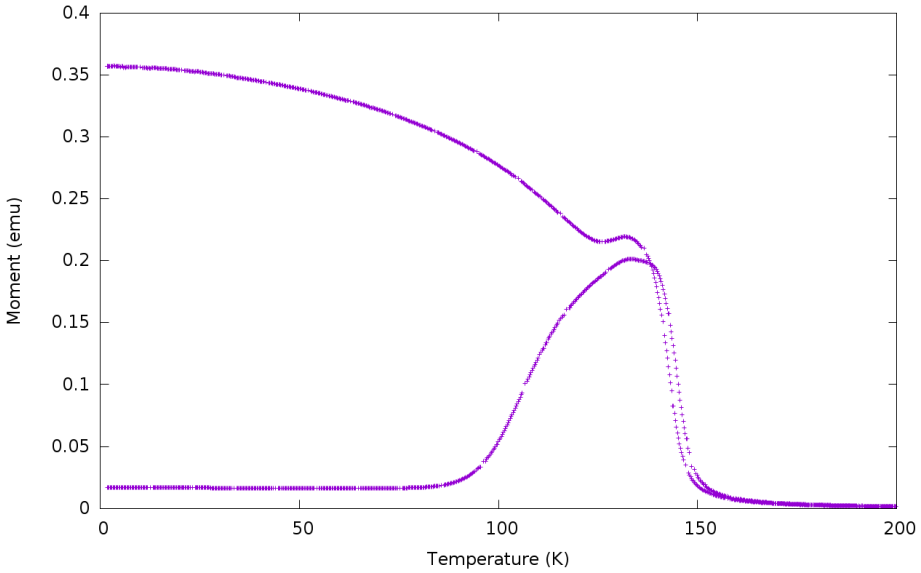

Fig. 6.10 ZFC and FC measurements of the UFe_4Al_8 sample with a field of 100 Oe.

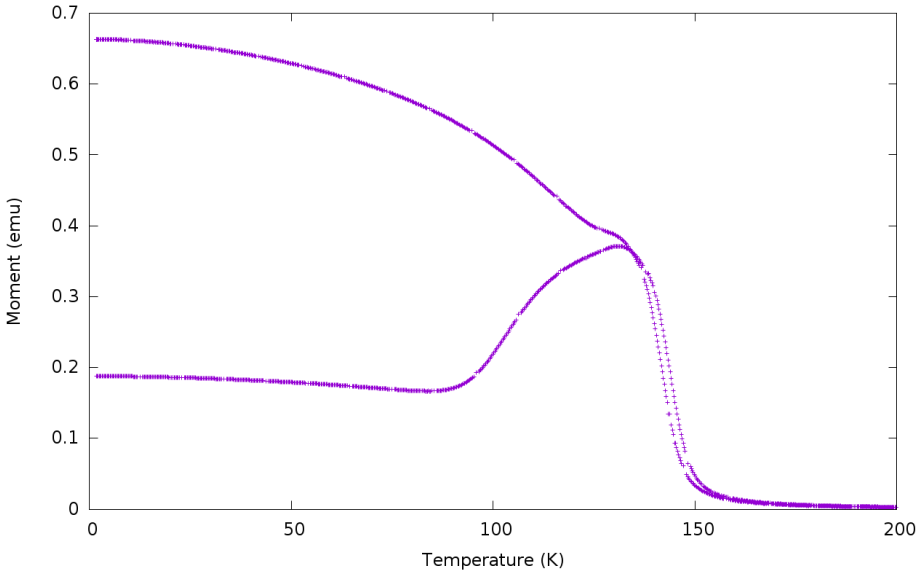

Fig. 6.11 ZFC and FC measurements of the UFe_4Al_8 sample with a field of 200 Oe.

The most important aspect is that DC measurements show the presence of only one peak, while in AC measurements two peaks can be distinguish in both real and imaginary component.

At higher frequencies the double peak appears to be split at even more peaks. This shows that AC susceptibility can give extra information than DC measurements, and can disclose details that are often missed in DC mode, as can be seen in Fig. 6.14.

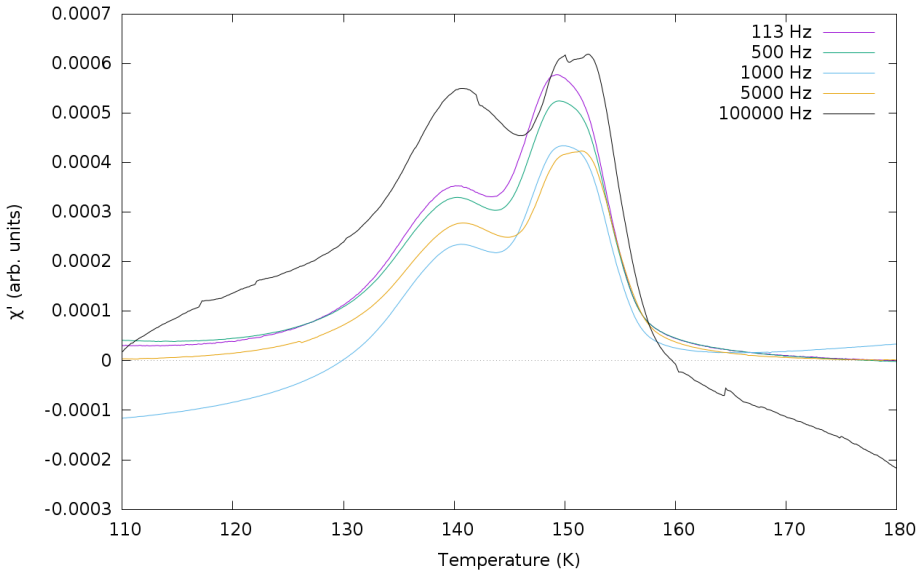

Fig. 6.12 UFe_4Al_8 AC real component.

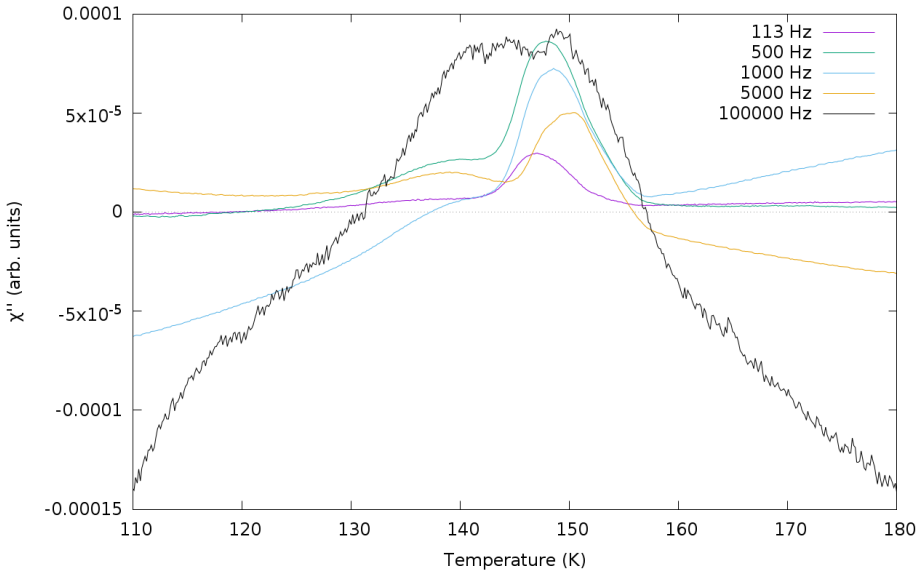

Fig. 6.13 UFe_4Al_8 AC imaginary component.

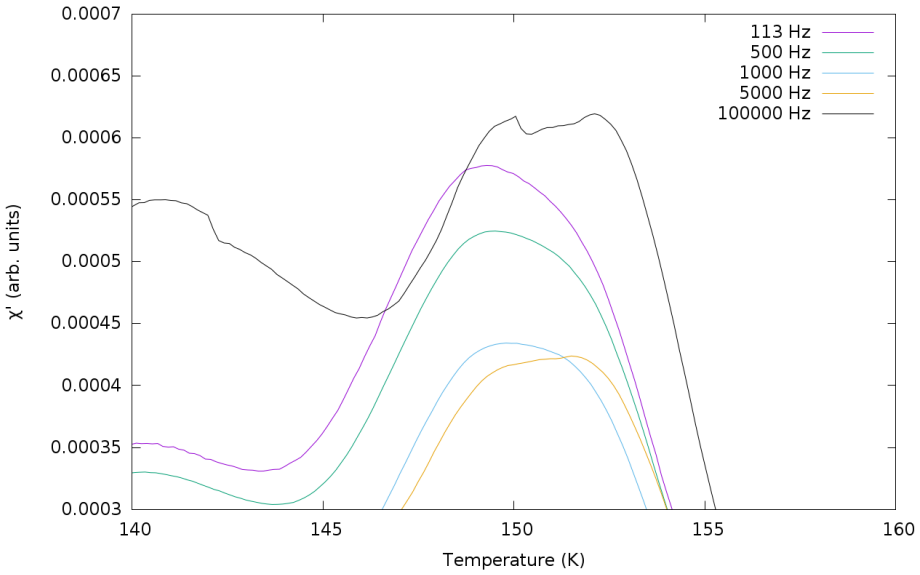

Fig. 6.14 UFe_4Al_8 AC real component peaks showing one more split than in DC measurements.

Chapter 7

Conclusions and Future Work

The susceptometer developed in this project revealed a high sensitivity to the measured signals, detecting small changes that were not present in *VSM* measurements. Due to the use of a lock-in amplifier, the sensitivity of the instrument is high and at the same time the measurements show low-noise, even in a relatively noisy environment. Of course the instrument will not reject the noise that exists in the narrow band of the lock-in amplifier filter, choosing the working frequencies of the susceptometer away from the most noisy sources (line frequency, mostly) is a must.

Although the system has a good sensitivity when it concerns to susceptibility, thermal contact between the sample and the coil interior surface is still not optimal, and an improvement on this issue should be envisaged. An absolute calibration of the instrument using a paramagnetic sample (typically Dy_2O_3) was not done due to time constraints and also to the fact that phase and background drift problems should be better tackled before embarking into such delicate absolute calibration. This is a project for future development. In either case, it should be stressed that most typical uses of AC magnetometry do not require absolute calibration and it is common to report AC measurements in arbitrary units.

As for the coil, new configurations were thought and a better one should be used in the production of a next-generation coil system, properly adapted to measurements of even smaller samples and with a higher surface contact with the sample holder to improve thermal contact.

Last but not least, a simple system should be implemented to monitor the current flow in the coil (or use a current source) so that a better phase adjustment is achieved, taking into account the dependence of the coil resistivity with temperature. Such a system is implemented on the AC susceptometer recently reported by Yonezawa et al [15].

References

[1] Agilent Technologies (2008). *INSTRUCTION MANUAL for TPS-compact*.

[2] de Waele, A. (2011). Basic operation of cryocoolers and related thermal machines. *Journal of Low Temperature Physics*, 164(5-6):179–236.

[3] Graham, C.D. (2000). High-sensitivity magnetization measurements. *Journal of Materials Science and Technology*, 16(2):97–101.

[4] Griffiths, D. (1999). *Introduction to Electrodynamics*. Prentice Hall.

[5] Lake Shore Cryotronics Inc. (2014). *User's Manual Model 335 Temperature Controller*.

[6] Laurent, P., Fagnard, J. F., Vanderheyden, B., Babu, N. H., Cardwell, D. A., Ausloos, M., and Vanderbemden, P. (2008). An ac susceptometer for the characterization of large, bulk superconducting samples. *Measurement Science and Technology*, 19(8):085705.

[7] Martien, D. (2002). Introdution to: Ac susceptibility.

[8] McElfresh, M. (1994). *Fundamentals of Magnetism and Magnetic Measurements*. Quantum Design.

[9] Nikolo, M. (1995). Superconductivity: A guide to alternating current susceptibility measurements and alternating current susceptometer design. *American Journal of Physics*, 63(1):57–65.

[10] Paixao, J., Lebech, B., Goncalves, A., Brown, P., Lander, G., Burlet, P., Delapalme, A., and Spirlet, J. (1997). Magnetic sublattice interactions in ufe4al8. *Physical Review B Condensed Matter*, 55(21):14370–14377.

[11] Quantum Design (2003). *AC Measurement System (ACMS) Option User's Manual*.

[12] Stanford Research Systems (2011). *Model SR830 DSP Lock-In Amplifier*.

[13] Ventura, G. , Risegari, L. (2008). *The Art of Cryogenics: Low-temperature Experimental Techniques*. Elsevier.

[14] Wurlitzer, M., Lorenz, M., Zimmer, K., and Esquinazi, P. (1997). ac susceptibility of structured $YBa_2Cu_3O_7$ thin films in transverse magnetic ac fields. *Phys. Rev. B*, 55:11816–11822.

[15] Yonezawa, S., Higuchi, T., Sugimoto, Y., Sow, C., and Maeno, Y. (2015). Compact ac susceptometer for fast sample characterization down to 0.1 k. *Review of Scientific Instruments*, 86(9).

Appendix A

Poster

In this appendix is a Poster presented during the academic year of the project.

DEVELOPMENT OF A CRYOGENIC MINIATURE AC-SUSCEPTOMETER FOR MAGNETIC PHASE TRANSITION IDENTIFICATION

F.J.P. Almeida,* J.A. Paixão*
*CEMDRX, Department of Physics, University of Coimbra

INTRODUCTION

Magnetic DC and AC susceptometry measures the response of materials to an applied magnetic field. The difference from DC to AC susceptometry is that, in the latter, the applied field varies in time, with a constant frequency. ACS had a big impact when *high* T_c superconductors were discovered, being still one of the best methods to characterize these materials. Not only superconductor transitions, but other magnetic transitions can also be identified with this method, that is very sensitive and reliable even with small samples that have low response.

AC SUSCEPTIBILITY

Magnetic susceptibility is the ratio $\chi = M/H$ where M is the sample magnetization in the applied magnetic field H, that can be measured in a DC experiment. If we apply an AC field, and as long as the field is small, the induced AC moment is

$$M_{\mathrm{AC}} = \frac{dM}{dH} \cdot H_{\mathrm{AC}} \sin(\omega t) \qquad (1)$$

where H_{AC} is the amplitude of the driving field, ω is the driving frequency, and $\chi = dM/dH$ is the slope of the $M(H)$ curve, the so called differential, dynamic or AC susceptibility. [1]
This susceptibility can be expressed as

$$\chi = \chi' + i\chi'' \qquad (2)$$

where χ' is the real component, which is related to the magnetic properties of the sample, and χ'' is the imaginary component of susceptibility, that is associated with the power density absorbed in the sample, given by

$$p_{\mathrm{av}} = \frac{1}{2}\mu_0 \omega H_0^2 \chi''. \qquad (3)$$

Both components can be determined from the magnitude, χ, and phase difference, θ, between the induced AC field and the measured response of the sample.

ACKNOWLEDGEMENTS

This work was supported by funds from FEDER (Programa Operacional Factores de Competitividade COMPETE) and from FCT-Fundação para a Ciência e Tecnologia under the project PEst-C/FIS/UI0036/2014. Access to TAIL-UC facility funded under QREN-Mais Centro Project ICT_2009_02_012_1890 is gratefully acknowledged.

REFERENCES

[1] MARTIEN, D. (2002). *AC Magnetic Measurements.* Quantum Design.
[2] NIKOLO, M. *Superconducivity: A guide to alternating current susceptibility measurements and alternating current susceptometer design.* Am. J Phys. **63**, 65 (1995).
[3] PAIXÃO, J.A., et.al. *Magnetic sublattice interactions in* UFe_4Al_8. Phys. Rev. B **55**, 14370 (1997).

SUSCEPTOMETER

AC susceptometers are based on a coil system that comprises a primary field coil (solenoid) and two coaxial secondary pick-up coils used to measure the ACS signal.[2] These pick-up coils are identical and connected in series opposition. In this case, if a sinusoidal current is passed through the primary coil, the voltage induced across the pick-up coils is nearly zero without sample. If the sample is placed in one of the pick-up coils a net voltage having the same frequency as the primary current will appear which is measured employing a lock-in amplifier (LIA).

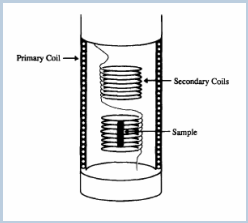

Figura 1: Susceptometer coils

We are desiging an instrument with a miniature coil system that can be placed in the cold finger of a closed cycle hellium cryostat.

EXPERIMENTAL SETUP

We are currently testing a protoype with coils with length of 2.5 cm and 1.5 cm diameter. The cryogenic system is an ARS closed cycle helium cryostat, working in a temperature range between 6 K and 350 K. The temperature close to the sample is measured with a miniature silicon diode thermometer. Data aquisition is based on a SRS830 LIA ($f_{\max} = 100\,\mathrm{kHz}$). The instrument is driven by a Python program providing also data analysis and ploting of results.

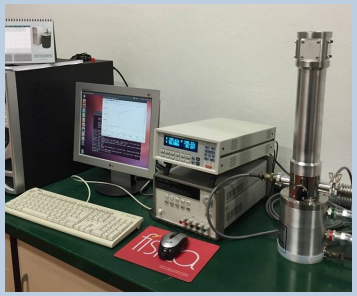

Figura 2: Closed cycle helium cryostat and temperature control module of the AC susceptometer

PHASE TRANSITIONS

To test the system in a wide temperature range, we have choosen to measure the transitions in Gd metal (ferromagnetic), UFe_4Al_8 (ferrimagnetic) and YBaCuO (superconductor).

Gadolinium is ferromagnetic with a Curie temperature close to room temperature (292 K). Both the real and imaginary components of the susceptibility are sensitive to the transition, the imaginary part arising from the dissipative motion of the magnetic domains in the sample.

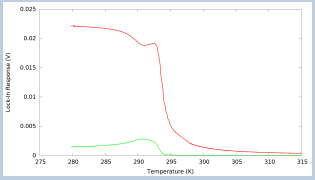

Figura 4: Gadolinium Susceptibility

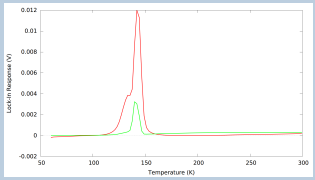

Figura 3: UFe4Al8 Susceptibility

The AC susceptibility in UFe_4Al_8 clearly shows the ordering of the two magnetic lattices around 150 K. The structure is ferrimagnetic with a weak ferromagnetic component in both the U and Fe atoms. [3]

YBaCuO shows the sharp superconducting transition at 92 K, visible in χ' (Meissner effect) and χ'' (lagging relative to χ') due to dissipative processes in the intergranular matrix.

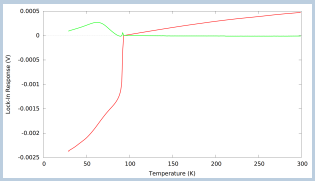

Figura 5: YBaCuO Susceptibility

FUTURE WORK

For the next step of this project, a new, highly sensitive set of coils are being designed with smaller fingerprint in the cryostat that should enable a wide range of systems to be studied, ranging from spin-glasses to molecular magnets.

Fig. A.1 Poster presented at 41st Conference on Phase Equilibria in Coimbra, Portugal